1994

Two-dimensional transport model for variably saturated porous meda with major ion chemistry

Jiří Šimůnek
USDA-ARS

Donald L. Suarez
USDA-ARS, donald.suarez@ars.usda.gov

WATER RESOURCES RESEARCH, VOL. 30, NO. 4, PAGES 1115–1133, APRIL 1994

Two-dimensional transport model for variably saturated porous media with major ion chemistry

Jiří Šimůnek[1] and Donald L. Suarez

U.S. Salinity Laboratory, Agricultural Research Service, U.S. Department of Agriculture, Riverside, California

Abstract. We present the development and demonstrate the use of the two-dimensional finite element code UNSATCHEM-2D for modeling major ion equilibrium and kinetic nonequilibrium chemistry in variably saturated porous media. The model is intended for prediction of major ion chemistry and water and solute fluxes for soils under transient conditions. Since the solution chemistry in the unsaturated zone is significantly influenced by variations in water content, temperature, and CO_2 concentrations in the soil gas, all these variables are also calculated by the model. The major variables of the chemical system are Ca, Mg, Na, K, SO_4, Cl, NO_3, alkalinity, and CO_2. The model accounts for equilibrium chemical reactions between these components such as complexation, cation exchange, and precipitation-dissolution. For the precipitation-dissolution of calcite and dissolution of dolomite, either equilibrium or multicomponent kinetic expressions are used which include both forward and back reactions. Other dissolution-precipitation reactions considered include gypsum, hydromagnesite, and nesquehonite. Since the ionic strength of soil solutions can often reach high values, both modified Debye-Hückel and Pitzer expressions were incorporated into the model to calculate single ion activities. The need for an iterative coupling procedure between the solute transport and chemical modules is demonstrated with an example which considers root water uptake and irrigation using moderatcly saline water. The utility of the model is further illustrated with two-dimensional simulations with surface and subsurface irrigation from a line source.

1. Introduction

Modeling the transport and chemical reactions of major solute species in and below the root zone plays a critical role for proper irrigation, fertilization, and surface and groundwater management. Realistic modeling of the root zone chemistry requires consideration of water flow and heat transport, as well as prediction of the dynamic changes in CO_2 concentration with time and space. It must also account for solute movement and the chemical processes for the solutes of interest. Soil temperature, which can change annually from about $-10°$ up to $+50°C$, significantly affects the thermodynamic equilibrium constants and reaction rates and therefore influences even the selection of the method for prediction of soil solution chemistry from equilibrium models to models based on kinetic expressions. In addition, CO_2 concentrations can change several orders of magnitude from values which are at equilibrium with the CO_2 content in the atmosphere (0.035%) up to extreme values of about 20%. The solubility of many solid phases such as carbonates and oxihydroxides significantly change within this range in CO_2 primarily because changes in soil CO_2 produce changes in soil pH for all but acid soils.

The processes of evaporation and plant transpiration also exert a major influence on the solution composition and water and solute distribution in near surface environments. These processes concentrate salts by decreasing the amount of water in the soil and when combined with irrigation in arid regions, saline conditions can result. Ion activities for such chemical conditions should be calculated with expressions suitable for use in brines rather than the standard formulations for dilute solutions. The interaction of evapotranspiration, changing soil gas composition, ion exchange, and soil water reactions requires consideration of the possibility to precipitate or dissolve various minerals. These major ions (consisting mainly of Ca^{2+}, Mg^{2+}, Na^+, K^+, Cl^-, SO_4^{2-}, HCO_3^-, CO_3^{2-}, and NO_3^-) may accumulate in certain parts of the soil profile in such amounts that crop yield can be seriously reduced. Therefore any model attempting to predict the solution chemistry of the major ions in the unsaturated zone should address all these processes and variables.

The hydrological models for water flow and solute transport and the chemical models considering solution chemistry were developed separately. The solute transport models mostly considered only one solute and simplified different chemical processes. The complex processes of adsorption and cation exchange were usually accounted for by linear [*Huyakorn et al.*, 1991] or nonlinear Freundlich isotherms [*Yeh and Huff*, 1985; *Šimůnek and van Genuchten*, 1993], where all reactions between solid and liquid phases were lumped into the distribution coefficient K_D [*Liu and Narasimhan*, 1989a] and possibly into the nonlinear exponent. Other processes such as precipitation, biodegradation, volatilization, or radioactive decay were simulated by simple developed which simulate several solutes involved in se-

[1]On leave from Research Institute for Soil Reclamation and Protection, Prague.

Paper number 93WR03347.

quential first-order decay reactions [*Gureghian*, 1981; *Wagenet and Hutson*, 1987; *Šimůnek and van Genuchten*, 1993].

Only in the last decade has there been significant effort to couple hydrological models for water flow and solute transport with chemical equilibrium models. Recent reviews on the development of the hydrogeochemical transport models of reactive multichemical components were given by *Abriola* [1987], *Kirkner and Reeves* [1988], *Yeh and Tripathi* [1989], *Rubin* [1990], and *Mangold and Tsang* [1991]. *Kirkner and Reeves* [1988] presented an analysis of several methods for approximate solution of multicomponent transport with homogeneous and heterogeneous chemical reactions and discussed how the nature of the chemistry may affect the choice of the numerical formulation and solution algorithm. *Yeh and Tripathi* [1989] provided a critical review of many computational methods that have been presented in the hydrologic literature for solving multicomponent, equilibrium-controlled transport.

Most of the research has been, and still is, concentrated on the saturated zone where changes in water velocity, temperature, and *p*H are relatively gradual and thus are less important than in the unsaturated zone. Therefore most of the developed models were based on one-dimensional steady state saturated water flow with fixed water velocity, temperature, and *p*H [e.g., *Valocchi et al.*, 1981; *Jennings et al.*, 1982; *Walsh et al.*, 1984; *Cederberg et al.*, 1985; *Kirkner et al.*, 1985; *Förster*, 1986; *Bryant et al.*, 1986; *Förster and Gerke*, 1989; *Kirkner and Reeves*, 1988]. Only recently several models were published that can be applied to problems that include multicomponent solute transport and two-dimensional variably saturated water flow [*Liu and Narasimhan*, 1989a; *Yeh and Tripathi*, 1991]. For example, *Narasimhan et al.* [1986] and *Liu and Narasimhan* [1989a] developed the model DYNAMIX that was coupled with an integral finite difference program for fluid flow in variably saturated porous media. *Yeh and Tripathi* [1991] presented the development and demonstration of a two-dimensional finite element hydrogeochemical transport model, HYDROGEOCHEM, for simulating transport of reactive multispecies chemicals. The presented examples in all these reports are only for steady state water movement.

Modeling of major ion chemistry in the soil profile, however, requires the coupling of a chemical model to a transient variably saturated water flow model which allows the simulation of such processes such as root water uptake. *Robbins et al.* [1980a, b] developed chemical precipitation-dissolution and cation exchange subroutines using equilibrium chemistry and coupled them with a one-dimensional water movement–salt transport–plant growth model. They tested their model by comparing its results with experimental data obtained from a lysimeter study. Further evaluation of their model was done by *Dudley et al.* [1981] for field conditions under cropped and uncropped conditions. They reported that the model gave adequate simulation of salinity but not individual ion concentrations. *Russo* [1986] combined the salinity model of *Robbins et al.* [1980a] with the transport model of *Bresler* [1973] to theoretically investigate the leaching of gypsiferous-sodic soil under different soil conditions and water qualities. Robbins' equilibrium chemistry model was also the basis for the numerical code LEACHM of *Hutson and Wagenet* [1992]. The main difference between LEACHM and the previous models is that they call the equilibrium chemistry model only once at each time step without iterating between transport and chemical modules. In many cases, as was shown by *Yeh and Tripathi* [1991] and as we will demonstrate in our first example, this simplification produces noticeable numerical error. The second limitation is that these models consider only equilibrium reactions, while published data in natural systems have indicated that kinetic reactions often control solution composition. For example, studies of major ion compositions in and below the root zone of calcareous arid zone soils have indicated that calcite equilibrium is not a reasonable assumption for predicting water composition [*Suarez*, 1977; *Suarez and Rhoades*, 1982] and that a kinetic expression yields values closer to the field measurements [*Suarez*, 1983]. Existing models also assume either a fixed *p*H or a fixed CO_2, which are questionable assumptions for soils, which usually exhibit fluctuation of both of these variables [*Suarez and Šimůnek*, 1993].

Modeling of CO_2 spatial distribution has been limited and has been attempted mostly by statistical correlation with specific parameters. The existing nonempirical models are mostly based on the assumption that the principal transport mechanism for CO_2 is molecular diffusion [*van Bavel*, 1951; *de Jong and Schappert*, 1972; *Solomon and Cerling*, 1987] and do not consider other transport mechanisms nor the influence of changes in water content and the dissolution of CO_2 in the liquid phase. Only recently, *Šimůnek and Suarez* [1993] developed a one-dimensional CO_2 transport model which considers CO_2 transport in both liquid and gaseous phases, as well as the biological production of CO_2.

Our main objectives in this paper are to develop and demonstrate a two-dimensional finite element model, UNSATCHEM-2D, for the modeling of major ion equilibrium and kinetic nonequilibrium chemistry in variably saturated porous media. Since, as mentioned above, the unsaturated zone chemistry is significantly influenced by variations in water content, temperature and CO_2 concentrations in the soil gas, the modeling of all these variables is included into UNSATCHEM-2D by coupling the two-dimensional version of the unsaturated water flow and solute transport code SWMS_2D of *Šimůnek et al.* [1992] with the CO_2, heat, and multicomponent solute transport. We do not give the details for the heat transport part of the model in this paper; however, it is available in the program documentation of UNSATCHEM-2D [*Šimůnek and Suarez*, 1994]. In this model we define Ca, Mg, Na, K, SO_4, Cl, NO_3, alkalinity, and CO_2 as major variables of the chemical system. The model accounts for equilibrium chemical reactions between these components such as complexation, cation exchange, and precipitation-dissolution. Ion exchange and equilibrium complexation are considered as instantaneous processes. For the precipitation-dissolution of calcite and dissolution of dolomite either equilibrium or multicomponent kinetic expressions can be used which include both forward and back reactions. Other dissolution-precipitation reactions considered include minerals gypsum, hydromagnesite, and nesquehonite. The ionic strength of soil solutions can vary considerably with time and space and often reach high values; thus both modified Debye-Hückel and Pitzer equations are incorporated into the model to calculate individual ion activities.

The model development and description is divided into sections. The model development is presented in the section ment solute transport. The second section also contains the

description of the chemical system together with the nonlinear algebraic equations characterizing this system. Section 3 discusses the numerical solution of the partial differential equations for water flow and solute transport, as well as the solution of the set of nonlinear algebraic equations of the chemical system. Coupling between solute transport and chemical modules is discussed in that section as well. In the fourth section we present two problems and the model simulations. A one-dimensional irrigation problem is used to illustrate the necessity to iterate between the chemical and solute transport modules and to compare results for the simulations with equilibrium and kinetic calcite precipitation. The two-dimensional problem is used to demonstrate the different water and solute profiles, including the chemical precipitation patterns, for surface and subsurface line irrigation.

2. Model Development

2.1. Variably Saturated Water Flow

2.1.1. Governing flow equation. Two-dimensional isothermal Darcian flow of water in a variably saturated rigid porous medium can be described by a modified form of the Richards equation under the assumptions that the air phase plays a negligible role in the liquid flow process and that the compressibility of both soil matrix and fluid can be ignored:

$$\frac{\partial \theta}{\partial t} = \frac{\partial}{\partial x_i}\left[K\left(K_{ij}^A \frac{\partial h}{\partial x_j} + K_{iz}^A\right)\right] - S \tag{1}$$

where θ is the volumetric water content $[L^3L^{-3}]$, h is the pressure head $[L]$, S is a sink term $[T^{-1}]$, x_i $(i = 1, 2)$ are the spatial coordinates $[L]$, t is time $[T]$, K_{ij}^A are components of a dimensionless anisotropy tensor $\mathbf{K}^A$, and K is the unsaturated hydraulic conductivity function $[LT^{-1}]$ given by

$$K(h, x, z) = K_s(x, z)K_r(h, x, z) \tag{2}$$

where K_r is the relative hydraulic conductivity [dimensionless] and K_s is the saturated hydraulic conductivity $[LT^{-1}]$. The anisotropy tensor K_{ij}^A in (1) is used to account for an anisotropic medium. The diagonal entries of K_{ij}^A equal one and the off-diagonal entries zero for an isotropic medium. Einstein's summation convention is used in (1) and throughout this paper.

2.1.2. Root water uptake. The sink term S in (1) represents the volume of water removed per unit time from a unit volume of soil due to plant water uptake. The expression proposed by *Feddes et al.* [1978] and subsequently modified to include the salinity stress [*Šimůnek and Suarez*, 1993] is

$$S(h) = a(h)a_\phi(h_\phi)S_p \tag{3}$$

where the water and salinity stress response functions $a(h)$ and $a_\phi(h_\phi)$ are prescribed dimensionless functions of the soil water pressure head h and osmotic head h_ϕ $(0 \le a \le 1)$, respectively, and S_p is the potential water uptake rate $[T^{-1}]$ which is equal to the water uptake rate during periods of no water and salinity stress when $a(h) = a_\phi(h_\phi) = 1$. The potential water uptake rate can be nonuniformly distributed over a root zone Ω_R of arbitrary shape as described in *Vogel* from the osmotic coefficient as described by D. L. Suarez and J. Šimůnek (Modeling major ion equilibrium and kinetic chemistry coupled to unsaturated water flow and solute transport, submitted to *Soil Science Society of America Journal*, 1994; hereinafter SS (1994)).

2.1.3. Unsaturated soil hydraulic properties. The unsaturated soil hydraulic properties are described by a set of closed-form equations of *van Genuchten* [1980], where the soil water retention function is given by

$$\theta(h) = \theta_r + \frac{\theta_s - \theta_r}{(1 + |\alpha h|^n)^m} \tag{4}$$

The hydraulic conductivity function is based on the capillary model of *Mualem* [1976]

$$K(h) = K_s S_e^{1/2}[1 - (1 - S_e^{1/m})^m]^2 \tag{5}$$

where θ_r and θ_s denote residual and saturated moisture content $[L^3L^{-3}]$, respectively, S_e is relative saturation [dimensionless], and m [dimensionless], n [dimensionless], and α $[L^{-1}]$ are the parameters of the hydraulic characteristics.

2.1.4. Initial and boundary conditions. The solution of (1) requires knowledge of the initial distribution of the pressure head within the flow domain Ω

$$h(x, z, 0) = h_i(x, z) \tag{6}$$

where h_i is a prescribed function of x and z.

Three types of conditions can be implemented to describe system-independent interactions along the boundaries of the flow region. These conditions are specified pressure head (Dirichlet type) boundary conditions of the form

$$h(x, z, t) = h_0(x, z, t) \qquad (x, z) \in \Gamma_D \tag{7}$$

specified flux boundary conditions given by

$$-\left[K\left(K_{ij}^A \frac{\partial h}{\partial x_j} + K_{iz}^A\right)\right]n_i = q_0(x, z, t) \qquad (x, z) \in \Gamma_F \tag{8}$$

and specified gradient (Neumann type) boundary conditions

$$\left(K_{ij}^A \frac{\partial h}{\partial x_j} + K_{iz}^A\right)n_i = g_0(x, z, t) \qquad (x, z) \in \Gamma_N \tag{9}$$

where Γ_D, Γ_F, and Γ_N indicate Dirichlet, flux, and Neumann type boundary segments, respectively; h_0, q_0, and g_0 are prescribed functions of x, z, and t; and n_i are the components of the outward unit vector normal to the boundary Γ_F or Γ_N.

In addition to the system-independent boundary conditions given by (7), (8), and (9), two types of system-dependent boundary conditions which depend on the prevailing (transient) soil moisture conditions close to the boundary can be specified. These include soil-air interfaces which are exposed to atmospheric conditions and seepage faces. For details on these boundary conditions see, for example, *Neuman et al.* [1974] or *Šimůnek et al.* [1992].

2.2. Multicomponent Solute Transport

2.2.1. Governing solute transport equation. Rigorous species requires several refinements to Fick's laws. Actual

diffusion rates are influenced by the effects of Coulomb interactions which maintain electroneutrality and which lead to a coupling between each solute flux and all concentration gradients [*Lasaga*, 1979]. Ion pairing (see section 2.4) represents another coupling mechanism, since it couples the fluxes of the particular ions in a special way, as is described by *Lasaga* [1979]. Nevertheless, these refinements to Fick's laws go beyond the scope of this paper and will not be considered here. This assumption is required only for cases where diffusion is the dominant process for solute transport.

The partial differential equation governing two-dimensional advective-dispersive chemical transport under transient water flow conditions in partially saturated porous media is taken as

$$\frac{\partial(\theta c_k)}{\partial t} + \rho \frac{\partial \bar{c}_k}{\partial t} + \rho \frac{\partial \hat{c}_k}{\partial t} = \frac{\partial}{\partial x_i}\left(\theta D_{ij} \frac{\partial c_k}{\partial x_j} - q_i c_k\right) \qquad (10)$$

$$k = 1, 2, \ldots, N_c$$

where c_k is the total dissolved concentration of the aqueous component k $[ML^{-3}]$, $\bar{c}_k$ is the total sorbed concentration of the aqueous component k $[MM^{-1}]$, $\hat{c}_k$ is the total precipitated concentration of aqueous component k $[MM^{-1}]$, ρ is the bulk density of the medium $[ML^{-3}]$, D_{ij} is the "effective" dispersion coefficient tensor $[L^2T^{-1}]$, q_i is the volumetric flux $[LT^{-1}]$, and N_c is the number of aqueous components. Solute uptake by plant roots is not considered in (10). The second and third terms on the left side of (10) are zero for components that do not undergo ion exchange or precipitation/dissolution.

Substituting the continuity equation which describes isothermal Darcian flow of water in a variably saturated porous medium

$$\frac{\partial \theta}{\partial t} = -\frac{\partial q_i}{\partial x_i} - S \qquad (11)$$

into the transport equation in a conservative form (10) we obtain the advective form of the transport equation

$$\theta \frac{\partial c_k}{\partial t} + \rho \frac{\partial \bar{c}_k}{\partial t} + \rho \frac{\partial \hat{c}_k}{\partial t} = \frac{\partial}{\partial x_i}\left(\theta D_{ij} \frac{\partial c_k}{\partial x_j}\right) - q_i \frac{\partial c_k}{\partial x_i} + S c_k \qquad k = 1, 2, \cdots, N_c \qquad (12)$$

The advective form of the transport equation was suggested to be more appropriate than the conservative form when using the finite element technique [*Huyakorn et al.*, 1985].

2.2.2. Dispersion coefficient. The components of the dispersion tensor D_{ij} in (10) are given by [*Bear*, 1972]

$$\theta D_{ij} = D_T |q| \delta_{ij} + (D_L - D_T) \frac{q_j q_i}{|q|} + \theta D_w \tau_w \delta_{ij} \qquad (13)$$

where D_w is the temperature dependent molecular diffusion coefficient in free water $[L^2T^{-1}]$, τ_w is a tortuosity factor in the dissolved phase $[LL^{-1}]$, $|q|$ is the absolute value of the Darcian fluid flux density $[LT^{-1}]$, δ_{ij} is the Kronecker delta function ($\delta_{ij} = 1$ if $i = j$, and $\delta_{ij} = 0$ *if* $i \neq j$), and D_L and respectively. The tortuosity factor is evaluated as a function of the water content using the relationship of *Millington and Quirk* [1961]:

$$\tau_w = \theta^{7/3}/\theta_s^2 \qquad (14)$$

2.2.3. Initial and boundary conditions. The solution of (12) requires knowledge of the initial concentration within the flow region Ω, i.e.,

$$c(x, z, 0) = c_i(x, z) \qquad (15)$$

where c_i is a prescribed function of x and z $[ML^{-3}]$. The index k is dropped to simplify the notation.

Two types of boundary conditions (Dirichlet and Cauchy type conditions) can be specified along the boundary of Ω. The first-type (or Dirichlet type) boundary conditions prescribe the concentration along a boundary segment Γ_D

$$c(x, z, t) = c_0(x, z, t) \qquad (x, z) \in \Gamma_D \qquad (16)$$

whereas third-type (Cauchy type) boundary conditions are used to prescribe the concentration flux along a boundary segment Γ_C as follows:

$$-\theta D_{ij} \frac{\partial c}{\partial x_j} n_i + q_i n_i c = q_i n_i c_0 \qquad (x, z) \in \Gamma_C \qquad (17)$$

in which $q_i n_i$ represents the outward fluid flux $[LT^{-1}]$, n_i is the outward unit normal vector [dimensionless], Γ_C indicates Cauchy type boundary segments, and c_0 is the concentration of the incoming fluid $[ML^{-3}]$. In some cases, for example when Γ_C is an impermeable boundary ($q_i n_i = 0$), or when water flow is directed out of the region, (17) reduces to a second-type (Neumann type) boundary condition of the form

$$\theta D_{ij} \frac{\partial c}{\partial x_j} n_i = 0 \qquad (18)$$

2.3. Carbon Dioxide Transport

2.3.1. Governing CO_2 transport equation. A detailed development of the one-dimensional carbon dioxide transport model and justification of respective assumptions were given by *Šimůnek and Suarez* [1993], and therefore we give here only the major equations without discussing all the details, such as the boundary conditions and all the specifics of the CO_2 production submodel.

We assumed that the CO_2 transport in the unsaturated zone occurs in both the liquid and gas phases. Furthermore, we considered that the CO_2 concentration in the soil is governed by two transport mechanisms [*Patwardhan et al.*, 1988], convective transport in the aqueous phase and diffusive transport in both gas and aqueous phases, and by CO_2 production and/or removal. Thus the two-dimensional CO_2 transport is described by the following mass balance equation

$$\frac{\partial(c_a\theta_a + c_w\theta)}{\partial t} = \frac{\partial}{\partial x_i}\left(\theta_a D_{ij}^a \frac{\partial c_a}{\partial x_j}\right) + \frac{\partial}{\partial x_i}\left(\theta D_{ij}^w \frac{\partial c_w}{\partial x_j}\right) - \frac{\partial}{\partial x_i}(q_i c_w) - S c_w + P \qquad (19)$$

the dissolved phase and gas phase $[L^3L^{-3}]$, respectively,

Table 1. Species Considered in the Chemical Submodel

	Group	Species
1	Aqueous components	Ca^{2+}, Mg^{2+}, Na^+, K^+, SO_4^{2-}, Cl^-, NO_3^-
2	Complexed species	$CaCO_3^0$, $CaHCO_3^+$, $CaSO_4^0$, $MgCO_3^0$, $MgHCO_3^+$ $MgSO_4^0$, $NaCO_3^-$ $NaHCO_3^0$, $NaSO_4^-$, KSO_4^-
3	Precipitated species	$CaCO_3$, $CaSO_4 \cdot 2H_2O$, $MgCO_3 \cdot 3H_2O$, $Mg_5(CO_3)_4(OH)_2 \cdot 4H_2O$, $CaMg(CO_3)_2$
4	Sorbed species	$\overline{Ca}$, $\overline{Mg}$, $\overline{Na}$, $\overline{K}$
5	CO_2-H_2O species	$CO_{2(g)}$, $H_2CO_3^*$, CO_3^{2-}, HCO_3^-, H^+, OH^-, H_2O

D_{ij}^a is the effective soil matrix diffusion coefficient tensor of CO_2 in the gas phase $[L^2T^{-1}]$, D_{ij}^w is the effective soil matrix dispersion coefficient tensor of CO_2 in the dissolved phase $[L^2T^{-1}]$, q_i is the soil water flux $[LT^{-1}]$, θ_a is the volumetric air content $[L^3L^{-3}]$, and P is the CO_2 production rate $[L^3L^{-3}T^{-1}]$. The term Sc_w represents the dissolved CO_2 removed from the soil by root water uptake; i.e., when plants take up water the dissolved CO_2 is also removed from the soil water system.

The volumetric concentrations of CO_2 in the dissolved and gas phases are related by the following equation:

$$c_w = K_c c_a \tag{20}$$

where K_c is the distribution constant which is strongly dependent on temperature [dimensionless]. *Šimůnek and Suarez* [1993] defined the total aqueous phase CO_2, c_w, as the sum of CO_2(aq) and H_2CO_3, and related it to the CO_2 concentration in the gas phase with Henry's law. However, aqueous carbon exists also as HCO_3^-, CO_3^{2-}, and other complexed species and these species should be included in the definition of c_w. Determination of these species cannot be made without use of a complete chemical speciation program. This calculation is performed in section 2.4, and the calculated c_w is used in (19).

Substituting (20) and the continuity equation which describes isothermal Darcian flow of water in a variably saturated porous medium (11) into the CO_2 transport equation in a conservative form (19) we obtained, again, the advective form of the transport equation

$$(\theta_a + \theta K_c)\frac{\partial c_a}{\partial t} = \frac{\partial}{\partial x_i}\left(\theta_a D_{ij}^a \frac{\partial c_a}{\partial x_j}\right) + \frac{\partial}{\partial x_i}\left(\theta_w D_{ij}^w \frac{\partial K_c c_a}{\partial x_j}\right) - q_i^w K_c \frac{\partial c_a}{\partial x_i} + F c_a + P \tag{21}$$

where

$$F = \frac{\partial \theta}{\partial t} - \theta \frac{\partial K_c}{\partial t} - q_i^w \frac{\partial K_c}{\partial x_i} \tag{22}$$

and which is further used for the numerical solution.

The effective dispersion coefficient in the liquid phase D_{ij}^w is defined similarly as in (13) and the effective diffusion coefficient in the gas phase D_{ij}^a is defined as

$$\theta_a D_{ij}^a = \theta_a D_a \tau_a \delta_{ij} \tag{23}$$

where D_a is the molecular diffusion coefficient of CO_2 in air $[L^2T^{-1}]$, which is calculated by (14) replacing water content with gas content. The temperature dependence of the molecular diffusion coefficients of CO_2 in air and water is taken from *Glinski and Stepniewski* [1985].

2.3.2. Production of carbon dioxide. Since processes other than biological ones are generally of relatively minor importance for CO_2 production in the soil, we did not include them into our model for CO_2 production. We classify CO_2 production into two processes: production by soil microbes and production by plant root respiration. We assume that the individual biological CO_2 production processes are additive and that it is possible to superpose individual mechanisms which reduce production from the optimal value [*Šimůnek and Suarez*, 1993]. The production of CO_2 is then considered as the sum of the production rate by the soil micoorganisms, $\gamma_s[L^3L^{-3}T^{-1}]$, and the production rate by plant roots, $\gamma_p[L^3L^{-3}T^{-1}]$:

$$P = \gamma_s + \gamma_p = \gamma_{s0}\prod_i f_{si} + \gamma_{p0}\prod_i f_{pi} \tag{24}$$

where the subscript s refers to soil microorganisms and the subscript p refers to plant roots, Πf_i is the product of reduction coefficients dependent on depth, temperature, pressure head (the soil water content), CO_2 concentration, osmotic head, and time. The parameters γ_{s0} and γ_{p0} represent the optimal CO_2 production by the soil microorganisms or plant roots, respectively, for the whole soil profile at 20°C under optimal water, solute, and CO_2 concentration conditions $[L^3L^{-2}T^{-1}]$. The individual reduction functions are given by *Šimůnek and Suarez* [1993], and the discussion of selection of the values for optimal production as well as coefficients for respective reduction functions is given in the work by *Suarez and Šimůnek* [1993].

2.4. Solution Chemistry

2.4.1. Elements of the chemical submodel. We assume that the chemical system for predicting major ion solute chemistry of the unsaturated zone includes 33 chemical species which can be divided into five groups as listed in Table 1. Seven chemical components (calcium, magnesium, sodium, potassium, sulfate, chloride, and nitrate), 10 complex aqueous species, five possible solid species (calcite, gypsum, nesquehonite, hydromagnesite, and dolomite), four sorbed species, and seven species which form the CO_2-H_2O system are considered. The species from the last group could be generally included in other groups (i.e., CO_3^{2-} and H^+ could be included in the first group). Their consideration as a separate group is mainly due to their different treatment during the numerical solution in comparison to that of the are considered as high ionic strength when using the proce

equations to calculate activity coefficients, while except for $CaCO_3^0$ and $MgCO_3^0$, the species of the second group are omitted as discussed later. The definitions of the terms component and species are those defined, for example, by *Westall et al.* [1976] and *Yeh and Tripathi* [1989]. Since, as is also discussed later, one of the solid phases (dolomite) is not included into the equilibrium system and its dissolution is always treated kinetically and the exclusion of the second solid phase (calcite) from the equilibrium system and its kinetic treatment is optional, we need, respectively, either 32 or 31 independent equations to solve this system. The phase rule is not violated, since only one magnesium solid can be present in the solution and this solid is determined by the model according to actual values of P_{CO_2}, (H_2O) and (H_2SiO_4). In the following sections we present these equations, and in section 3.2 we discuss the numerical solution method.

2.4.2. Mass and charge balance equations. Seven mass balance equations for the major constituents in the first group of Table 1 are defined:

$$Ca_T = [Ca^{2+}] + [CaSO_4^0] + [CaCO_3^0] + [CaHCO_3^-] \quad (25a)$$

$$Mg_T = [Mg^{2+}] + [MgSO_4^0] + [MgCO_3^0] + [MgHCO_3^-] \quad (25b)$$

$$Na_T = [Na^+] + [NaSO_4^-] + [NaCO_3^-] + [NaHCO_3^0] \quad (25c)$$

$$K_T = [K^+] + [KSO_4^-] \quad (25d)$$

$$SO_{4_T} = [SO_4^{2-}] + [CaSO_4^0] + [MgSO_4^0] + [NaSO_4^-] + [KSO_4^-] \quad (25e)$$

$$Cl_T = [Cl^-] \quad (25f)$$

$$NO_{3T} = [NO_3^-] \quad (25g)$$

where variables with subscript T represent the total analytical concentration in solution of that particular variable and where brackets refer to molalities (moles per kilogram). Two mass balance equations for the total analytical concentration of carbonate and bicarbonate are defined:

$$CO_{3T} = [CO_3^{2-}] + [CaCO_3^0] + [MgCO_3^0] + [NaCO_3^-]$$
$$HCO_{3_T} = [HCO_3^-] + [CaHCO_3^+] + [MgHCO_3^+] + [NaHCO_3^0] \quad (26)$$

which are used to calculate carbonate alkalinity (moles charge per kilogram) as

$$Alk = 2CO_{3_T} + HCO_{3_T} + [OH^-] - [H^+] \quad (27)$$

Most chemical and multicomponent transport models use the total inorganic carbon as a conservative property [e.g., *Westal et al.*, 1986; *Liu and Narasimhan*, 1989b; *Yeh and Tripathi*, 1991]. However, this approach can be used only for closed systems. In a soil environment with fluctuating CO_2 concentrations this approach is inappropriate, since changes in CO_2 produce changes in dissolved inorganic carbon. Use of alkalinity is therefore preferable, since alkalinity is conalkalinity nor total inorganic carbon are constant for systems where mineral precipitation or dissolution occurs. Total dissolved inorganic carbon as a sum of CO_{3T}, HCO_{3T}, $CO_2(aq)$, and H_2CO_3 is calculated as well to obtain the proper value of the distribution constant K_c for the CO_2 transport calculations (20).

In addition to the mass balance equations, the charge balance equation for the solution is given as

$$2[Ca^{2+}] + 2[Mg^{2+}] + [Na^+] + [K^+] + [CaHCO_3^+] + [MgHCO_3^+] + [H^+] - 2[CO_3^{2-}] - [HCO_3^-] - 2[SO_4^{2-}] - [Cl^-] - [NO_3^-] - [OH^-] - [NaCO_3^-] - [NaSO_4^-] - [KSO_4^-] = 0 \quad (28)$$

2.4.3. CO_2-H_2O system. The activities of the species present in solution at equilibrium are related by the mass action equilibrium equations. The dissociation of water is written as follows:

$$H_2O \rightleftarrows H^+ + OH^- \qquad K_w = \frac{(H^+)(OH^-)}{(H_2O)} \quad (29)$$

where K_w is the dissociation constant for water [dimensionless]. The parentheses denote ion activity, the calculation of which is discussed later.

The solubility of $CO_2(g)$ in water is governed by Henry's law:

$$H_2CO_3^* \rightleftarrows CO_{2(g)} + H_2O \qquad K_{CO_2} = \frac{(H_2CO_3^*)}{P_{CO_2}(H_2O)} \quad (30)$$

where the activity of $CO_{2(g)}$ is expressed in terms of the partial pressure P_{CO_2} (pascals), K_{CO_2} is Henry's law constant, and $H_2CO_3^*$ represents both aqueous CO_2 and H_2CO_3.

Protolysis reactions of dissolved CO_2 are written as

$$H_2CO_3^* \rightleftarrows H^* + HCO_3^- \qquad K_{a_1} = \frac{(H^+)(HCO_3^-)}{(H_2CO_3^*)} \quad (31)$$

$$HCO_3^- \rightleftarrows H^+ + CO_3^{2-} \qquad K_{a_2} = \frac{(CO_3^{2-})(H^+)}{(HCO_3^-)} \quad (32)$$

where K_{a1} and K_{a2} are the first and the second dissociation constants of carbonic acid [dimensionless], respectively.

2.4.4. Complexation reactions. Each complexation reaction for the species in the second group of Table 1 can be represented by the law of mass action:

$$K_1 = \frac{(Ca^{2+})(SO_4^{2-})}{(CaSO_4^0)} \qquad K_2 = \frac{(Ca^{2+})(CO_3^{2-})}{(CaCO_3^0)} \qquad K_3 = \frac{(Ca^{2+})(HCO_3^-)}{(CaHCO_3^+)} \quad (33)$$

$$K_4 = \frac{(Mg^{2+})(SO_4^{2-})}{(MgSO_4^0)} \qquad K_5 = \frac{(Mg^{2+})(CO_3^{2-})}{(MgCO_3^0)}$$

$$(Mg^{2+})(HCO_3^-)$$
$$(MgHCO_3^+)$$

$$K_7 = \frac{(Na^+)(SO_4^{2-})}{(NaSO_4^-)} \quad K_8 = \frac{(Na^+)(CO_3^{2-})}{(NaCO_3^-)}$$

$$K_9 = \frac{(Na^+)(HCO_3^-)}{(NaHCO_3^0)} \tag{35}$$

$$K_{10} = \frac{(K^+)(SO_4^{2-})}{(KSO_4^-)} \tag{36}$$

where K_i is the equilibrium constant of the ith complexed species [dimensionless].

2.4.5. Cation exchange selectivity. Partition between the solid exchange phase and the solution can be described by the Gapon equation [*White and Zelazny*, 1986]

$$K_{ij} = \frac{\bar{c}_i^{y+}}{\bar{c}_j^{x+}} \frac{(c_j^{x+})^{1/x}}{(c_i^{y+})^{1/y}} \tag{37}$$

where y and x are the valences of species i and j, respectively, and K_{ij} is the Gapon selectivity coefficient [dimensionless]. The absorption concentration is expressed in moles charge per kilogram of soil. It is assumed that the cation exchange capacity $\bar{c}_T$ (moles charge per kilogram of soi) is constant and independent of pH:

$$\bar{c}_T = \Sigma \bar{c}_i \tag{38}$$

In the case of exchange of four cations ($\bar{C}a$, $\bar{M}g$, $\bar{N}a$, and $\bar{K}$) we obtain the following system of equations:

$$\bar{c}_T = \bar{C}a^{2+} + \bar{M}g^{2+} + \bar{N}a^+ + \bar{K}^+ \tag{39}$$

$$K_{11} = \frac{\bar{M}g^{2+}}{\bar{C}a^{2+}} \frac{(Ca^{2+})^{1/2}}{(Mg^{2+})^{1/2}}$$

$$K_{12} = \frac{\bar{C}a^{2+}}{\bar{N}a^+} \frac{(Na^+)}{(Ca^{2+})^{1/2}} \tag{40}$$

$$K_{13} = \frac{\bar{C}a^{2+}}{\bar{K}^+} \frac{(K^+)}{(Ca^{2+})^{1/2}}$$

2.4.6. Precipitation-dissolution reactions. We consider three solid phases in our model which if specified or approached from oversaturation must be in equilibrium with the solution: gypsum, nesquehonite, and hydromagnesite. Precipitation-dissolution of calcite can be optionally treated with either equilibrium or kinetic expressions. In the latter case the equation corresponding to calcite equilibrium presented in this section is disregarded from the equilibrium system, and the rate of calcite precipitation-dissolution is calculated from the rate equation as described later. Dissolution of dolomite, which is also discussed later, is always considered as a kinetic process and never included into the equilibrium system, since true ordered dolomite does not precipitate under Earth surface conditions. Discussion on the selection and consideration of these solids is given in the work by SS (1994). The precipitation or dissolution of gypsum, calcite (if considered in equilibrium system), nesquehonite and hydromagnesite in the presence of CO_2 can be described by

$$CaSO_4 \cdot 2H_2O \rightleftarrows Ca^{2+} + SO_4^{2-} + 2H_2O \tag{41}$$

$$CaCO_3 + CO_2(g) + H_2O \rightleftarrows Ca^{2+} + 2HCO_3^- \tag{42}$$

$$MgCO_3 \cdot 3H_2O + CO_2(g) \rightleftarrows Mg^{2+} + 2HCO_3^- + 2H_2O \tag{43}$$

$$Mg_5(CO_3)_4(OH)_2 \cdot 4H_2O + 6CO_2(g) \rightleftarrows 5Mg^{2+} + 10HCO_3^- \tag{44}$$

with the corresponding solubility products K_{SP} [dimensionless]

$$K_{SP}^G = (Ca^{2+})(SO_4^{2-})(H_2O)^2 \tag{45}$$

$$K_{SP}^C = (Ca^{2+})(CO_3^{2-}) \tag{46}$$

$$K_{SP}^N = (Mg^{2+})(CO_3^{2-})(H_2O)^3 \tag{47}$$

$$K_{SP}^H = (Mg^{2+})^5(CO_3^{2-})^4(OH^-)^2(H_2O)^4 \tag{48}$$

where indexes G, C, N, and H refer to gypsum, calcite, nesquehonite, and hydromagnesite, respectively.

Substituting of (29) through (32) into (46) through (48) we get the solubility products for the carbonate solids expressed in terms of bicarbonate, which is the major carbonate ion under most natural conditions ($6.35 < p\text{H} < \sim 9.5$).

$$(Ca^{2+})(HCO_3^-)^2 = K_{SP}^C \frac{K_{CO_2} K_{a_1} P_{CO_2} (H_2O)}{K_{a_2}} \tag{49}$$

$$(Mg^{2+})(HCO_3^-)^2 = K_{SP}^N \frac{K_{CO_2} K_{a_1}}{K_{a_2}} \frac{P_{CO_2}}{(H_2O)^2} \tag{50}$$

$$(Mg^{2+})^5(HCO_3^-)^{10} = K_{SP}^H \frac{K_{CO_2}^6 K_{a_1}^6 P_{CO_2}^6}{K_{a_2}^4 K_w^2} \tag{51}$$

Expressing the solubility products in this way decreases significantly the number of iterations necessary to numerically reach equilibrium conditions, in comparison with using (46) through (48). The equilibrium concentrations of Ca^{2+} and SO_4^{2-} with gypsum can be obtained by solving the quadratic algebraic equation corresponding to (45). The equilibrium concentrations of Ca^{2+}, Mg^{2+}, and HCO_3^- with the carbonate solids is reached by solving the cubic algebraic equations corresponding to (49) through (51), as is described by SS (1994).

2.4.7. Kinetic model of calcite precipitation-dissolution. The reaction rates of calcite precipitation-dissolution in the absence of inhibitors such as "forcign ions" and dissolved organic matter (millimoles per square centimeter per second) can be calculated with the rate equation of *Plummer et al.* [1978]:

$$R^C = k_1(H^+) + k_2(H_2CO_3^*) + k_3(H_2O) - k_4 \frac{K_{a_2}}{K_{SP}^C} (Ca^{2+})(HCO_3^-) \tag{52}$$

where

$$(H_s^1)$$

and where k_1, k_2, and k_3 are temperature-dependent first-order rate constants representing the forward reactions (millimoles per square centimeter per second), and k_4 is a function dependent on both temperature and CO_2 concentration representing the back reactions (millimoles per square centimeter per second). The dissolution/precipitation rate R^c is expressed in mmol of calcite per square centimeter of surface area per second. The term (H_s^+) is the H^+ activity at the calcite surface; it is assumed to be (H^+) at calcite saturation where activities of $H_2CO_3^*$ and H_2O at the calcite surface are equal to their bulk fluid values [*Plummer et al.*, 1978]. The temperature dependence of the constants k_1, k_2, and k_3 is given by *Plummer et al.* [1978].

For the condition where $pH > 8$ and $P_{CO_2} < 1000$ Pa, the following expression for the precipitation rate, which is considered more accurate for those conditions [*Inskeep and Bloom*, 1985], is used:

$$R^c = -11.82[(Ca^{2+})(CO_3^{2-}) - K_{SP}^C] \tag{54}$$

with an apparent Arrhenius activation energy of 48.1 kJ mol^{-1} for the precipitation rate constant [*Inskeep and Bloom*, 1985].

The precipitation or dissolution rate of calcite is inhibited by the presence of different inhibitors. SS (1994) developed the following function for the reduction of the precipitation-dissolution rates due to surface poisoning by dissolved organic carbon, based on the experimental data of *Inskeep and Bloom* [1986]:

$$r = \exp(-b_1 x - b_2 x^2 - b_3 x^{0.5}) \tag{55}$$

where r is the reduction constant [dimensionless], x is the dissolved organic carbon (micromoles per liter), and b_1, b_2, and b_3 are regression coefficients (0.005104, 0.000426, 0.069111, respectively, with a r^2 value of 0.997).

2.4.8. Kinetic model of dolomite dissolution. The reaction rates of dolomite dissolution R^D (millimoles per square centimeter per second) are calculated with the rate equation of *Busenberg and Plummer* [1982]:

$$R^D = k_1(H^+)^{0.5} + k_2(H_2CO_3^*)^{0.5} + k_3(H_2O)^{0.5} - k_4(HCO_3^-) \tag{56}$$

where the temperature dependent first-order rate constants k_1, k_2, and k_3 (millimoles per square centimeter per second), representing the forward reactions, and k_4 (millimoles per square centimeter per second), representing the back reaction, are given by *Busenberg and Plummer* [1982]. The dissolution rate R^D is again expressed in millimoles of dolomite per square centimeter of surface area per second.

2.4.9. Activity coefficients. The solute activity coefficients are formally defined as [*Stokes*, 1979]

$$a_i = \gamma_i m_i / m^0 \tag{57}$$

where a_i is the activity [dimensionless], m_i is the molality (moles per kilogram), m^0 is the standard state unit molality (i.e., 1 mol kg^{-1}), and γ_i is the activity coefficient of the ith ion [dimensionless]. Calculation of the single ion activity coefficient can be specified either using an extended version of the Debye-Hückel equation [*Truesdell and Jones*, 1974] or version of the Debye-Hückel equation [*Truesdell and Jones*, 1974], which can be used in the dilute to moderately saline solution range, is given by

$$\ln \gamma = -\frac{Az^2\sqrt{I}}{1 + Ba\sqrt{I}} + bI \tag{58}$$

where A ($kg^{0.5}$ $mol^{-0.5}$) and B ($kg^{0.5}$ cm^{-1} $mol^{-0.5}$) are constants depending only on the dielectric constant, density, and temperature, z is the ionic charge, a (centimeters) and b (kilogram per mole) are two adjustable parameters, and I is the ionic strength (moles per kilogram):

$$I = 0.5 \sum_{i=1}^{M} z_i^2 m_i \tag{59}$$

where M is the number of species in the solution mixture. The adjustable parameters a and b for individual species are given by *Truesdell and Jones* [1974]. The activities of neutral species are calculated as

$$\ln \gamma = a' I \tag{60}$$

where a' is an empirical parameter (kilograms per mole). The values of this parameter for neutral species are listed in Table 2 in the work by SS (1994).

At high ionic strength, activity coefficients are no longer universal functions of ionic strength, but are dependent on the relative concentration of the various ions present in solution [*Felmy and Weare*, 1986]. The activity coefficients can then be expressed in a virial type expansion of the form [*Pitzer*, 1979]

$$\ln \gamma_i = \ln \gamma_i^{DH} + \sum_j B_{ij}(I) m_j + \sum_j \sum_k C_{ijk} m_j m_k + \cdots \tag{61}$$

where γ_i^{DH} is a modified Debye-Hückel activity coefficient which is a universal function of ionic strength [dimensionless], and B_{ij} and C_{ijk} are specific coefficients for each ion interaction. The specific forms of this equation for cations, anions, and neutral species are given in the appendix.

This model is considered accurate even for solutions with very high ionic strength (up to 20 m) and can be used down to infinite dilution. Explicit definition of most complex species (e.g., $NaSO_4^-$, $NaHCO_3^0$) for this type of model is generally not required [*Harvie et al.*, 1984]. However, ion complex species which exhibit strong attractive interactions (e.g., HCO_3^-), as well as $CaCO_3^0$ and $MgCO_3^0$, must still be taken into account. Therefore when the virial-type model is used to calculate ion activities, the complex species from the second group of Table 1 (except for $CaCO_3^0$ and $MgCO_3^0$) are not included into the equilibrium chemical system and the corresponding equations (33) through (36) are not used (again except for K_3 and K_5). The species in group five are considered even when the Pitzer expressions are utilized for activity coefficient calculations. Note that when the ion complex species from the second group in Table 1 are not considered, then the apparent ionic strength I increases significantly, since the complexes have lower charge than the original components.

The activity of water is calculated in accordance with the Hückel theory is used then the activity of water is calculated

as described by *Truesdell and Jones* [1974] by the approximate relation

$$(H_2O) = 1 - 0.017 \sum_{i=1}^{M} m_i \quad (62)$$

If the Pitzer theory is used then the activity of water is obtained from the expression [*Felmy and Weare*, 1986]

$$\ln (H_2O) = -\frac{W}{1000}\left(\sum_{i=1}^{M} m_i\right)\phi \quad (63)$$

where W is the molecular weight of water and ϕ is the osmotic coefficient (see *Felmy and Weare* [1986] for definition and method of calculation).

2.4.10. Temperature dependence. Most of the thermodynamic equilibrium constants are dependent on the temperature and pressure of the system. The temperature dependence of the thermodynamic equilibrium constants is often expressed as a power function of the absolute temperature

$$\log K = a_1 + a_2/T + a_3T + a_4 \log T + a_5T^2 \quad (64)$$

where T is the absolute temperature [K], and a_1 through a_5 are empirical constants. The pressure dependence is usually neglected under near Earth surface conditions. The empirical constants for the temperature dependent thermodynamic constants used in the calculations are listed in Table 3 of SS (1994). Temperature dependence of the equilibrium constants for which the constants of (64) do not exist is expressed with the enthalpy of reaction and the Van't Hoff expression [*Truesdell and Jones*, 1974].

2.4.11. System summary. As is discussed above, we need either 32 or 31 independent equations to solve the equilibrium system depending on whether calcite precipitation-dissolution is considered as a fast (instantaneous equilibrium) or slow (kinetic) process. Seven aqueous components of the first group in Table 1 are replaced by the mass balance equations (25). The analytical concentrations of the first six components are obtained from the solution of the solute transport equation (12), and the analytical concentration of the last component is obtained from the charge balance equation (28). Ten complexed species of the second group are replaced by (33) through (36). As is discussed above, this group is not completely considered when Pitzer virial-type expressions are used to calculate the ion activities. Precipitated species from the third group are replaced by (45) and (49) through (51), and sorbed species from the fourth group by (39) and (40). The CO_2 partial pressure is obtained from the carbon dioxide transport submodel and the activity of water is calculated by (62) or (63), depending on the method used to calculate activity coefficients. The last five species from the sixth group are replaced by (29) through (32) and the defining equation for alkalinity (27), which is also obtained from the solution of the transport equation. The whole system of equations is now mathematically closed.

3. Solution Strategy

3.1. Numerical Solution of Governing Transport Equations

The finite element method is used to obtain a solution of the water flow (1) and solute (12) and CO_2 (21) transport equations subject to the imposed initial and boundary conditions. Since the Galerkin method is relatively standard and has been covered in detail elsewhere [e.g., *Neuman*, 1975; *Pinder and Gray*, 1977; *Huyakorn and Pinder*, 1983] and since detailed description of the solution of Richards' equation (1) was given by *Šimnek et al.* [1992], only the most pertinent steps in the solution of the solute transport equation (12) will be given here. The "mass conservative" iterative method proposed by *Celia et al.* [1990] is used for evaluating the water content term in equation (1). Their method has been shown to provide excellent results in terms of minimizing the mass balance error. We do not discuss the numerical solution of the CO_2 transport equation (21), since it has a form similar to the solute transport equation.

Application of the standard Galerkin method to (12) leads to the following set of N equations:

$$\int_\Omega \left[-\theta \frac{\partial c}{\partial t} - q_i \frac{\partial c}{\partial x_i} + \frac{\partial}{\partial x_i}\left(\theta D_{ij} \frac{\partial c}{\partial x_j}\right) + Sc + G\right]\phi_n \, d\Omega = 0 \qquad n \in (1, N) \quad (65)$$

where

$$G = -\rho \frac{\partial \bar{c}}{\partial t} - \rho \frac{\partial \hat{c}}{\partial t} \quad (66)$$

Subscript k in the transport equation was omitted for simplicity. Application of Green's theorem to the second derivatives in (65) and subsequent substitution of a finite element approximation of c result in the system of time-dependent differential equations expressed in a matrix form as

$$[Q]\, d\{c\}/dt + [S]\{c\} + \{f\} = 0 \quad (67)$$

Integration of (67) in time is achieved by discretizing the time domain into a sequence of finite intervals and replacing the time derivatives by finite differences. The Crank-Nicholson finite difference scheme ($\varepsilon = 0.5$) is used for the transport equation

$$[Q]_{j+\varepsilon} \frac{\{c\}_{j+1} - \{c\}_j}{\Delta t_j} + \varepsilon[S]_{j+1}\{c\}_{j+1} + (1 - \varepsilon)[S]_j\{c\}_j + \varepsilon\{f\}_{j+1} + (1 - \varepsilon)\{f\}_j = 0 \quad (68)$$

where $j + 1$ denotes the current time level at which the solution is being considered, j refers to the previous time level, ε is a time weighing factor, and $\Delta t_j = t_{j+1} - t_j$. Since the coefficient vector f which contains the variable G (see (66)) is a function of the dependent variable c, the equations for solute transport are highly nonlinear. Evaluation of the term G in the solute transport equation is discussed in section 3.3. A more detailed description of the numerical solution of the solute transport equation is given by *Šimůnek and Suarez* [1994].

3.2. Solution of Chemical System

Computation of the solution species composition is accomplished in a fairly similar way as in the chemical model that does not consider sorption and precipitation. The mass

into the chemical submodel of UNSATCHEM-2D are the analytical concentrations of the major ions, alkalinity, adsorbed and solid phase concentrations, water content, temperature, bulk density of the soil, and CO_2 partial pressure. The submodel is divided into three major sections which have their own internal iteration criteria and which are coupled together by two additional global criteria. The global criteria are the test on electrical neutrality and on the ionic strength. All iteration criteria have a precision level of 0.1%.

The ionic strength, activity coefficients, and the temperature-dependent equilibrium constants are calculated initially using the specified model for the activity coefficients. Next, anionic weak acid species, carbonate-bicarbonate distribution, and pH are calculated and all solid phases considered in the equilibrium system are checked for their saturation index values and precipitated or dissolved (if present) accordingly. The iteration criterion in this section is the second dissociation constant of carbonic acid (see (32)).

The second section solves for ion pairs and complexes and consists of six subsections for calcium, magnesium, sodium, potassium, sulfate, and alkalinity. The iteration criterion inside of each subsection is the total analytical concentration of the respective variable. The main criterion for the whole section is again the second dissociation constant of carbonic acid.

The last section calculates the equilibrium between the soil solution and the adsorbed species. The iteration criterion in this section is the charge balance of free metal cations. After completion of the exchange calculations the global criteria are checked, and if not fulfilled, a new iteration is begun.

This whole process is accomplished for each node, at each time level, and each iteration between the solute transport part and equilibrium part of the model. When the *Plummer et al.* [1978] kinetic expressions for calcite are used the whole process is completed twice to obtain variables for the rate equation (52). First, we calculate the H^+ activity at the calcite surface with the assumption that activities of $H_2CO_3^*$ and H_2O at the calcite surface are equal to their bulk fluid values. This is accomplished by including calcite into the equilibrium system and excluding all other minerals and adsorbed species. During the second calculation, calcite is not considered as part of the equilibrium system and the calculated activities are used for calculation of the reaction rate.

3.3. Coupling Transport and Chemical Modules

The governing solute transport equation (12) contains three time derivative terms. The first is the time derivative of the total dissolved concentration of the aqueous component, and the second and the third are time derivatives of the sorbed and solid phase concentrations, respectively. For the numerical solution, the second and third terms are lumped together into the term G (see (66)). Because of this term, the solute transport equation (12) is highly nonlinear, and an iterative process must be applied to obtain its solution. Time changes of both the adsorbed and solid phase concentrations can be obtained directly from the chemical equilibrium submodel when all the reactions are considered as reaching equilibrium. When the kinetic expressions for the precipitation-dissolution of calcite and dolomite are used, the chemreactions. The contribution from the precipitation-dissolution reaction of calcite and dolomite to the time derivative of the solid phase concentration of a particular component can then be calculated as follows:

$$\rho\ \partial\hat{c}/\partial t = -R^C A^C - R^D A^D \tag{69}$$

where A^C and A^D are the surface areas of the calcite and dolomite per volume of soil [L^2L^{-3}], respectively.

Coupling between the transport and chemical submodules, which was described by *Walsh et al.* [1984], *Cederberg et al.* [1985], and *Bryant et al.* [1986], and was also used by *Yeh and Tripathi* [1990], is as follows. First, the discretized solute transport equation (68) is solved by setting the G term equal to zero for the equilibrium case or using (69) for the kinetic case. Then the new dissolved concentrations are compared with the initial concentrations for this iteration and the chemical module is called for those nodes where changes in concentrations were higher than some prescribed concentration tolerance. When the kinetic reactions for calcite or dolomite are used, then the chemical module is called for all nodes at the first iteration. The chemical module provides us with the updated values of aqueous, solid phase, and adsorbed concentrations and new values of the term G. The new aqueous concentrations are checked against those calculated before the chemical module was called and if different, a new iteration is started. This iteration process continues until the new and the old concentrations in all nodes differ less than some prescribed concentration tolerance.

4. Example Problems

The first of two examples considers one-dimensional vertical water flow and solute transport with steady boundary conditions. This example shows the prediction differences between the equilibrium and kinetic precipitation-dissolution model, as well as the importance of the iteration process between the solute transport and chemical modules. The second example demonstrates the use of UNSATCHEM-2D for a practical problem considering irrigation by surface and subsurface line irrigation. As demonstrated, these irrigation systems can cause development of saline zones which could subsequently cause unsuitable conditions for future seed germination and crop growth.

4.1. One-Dimensional Irrigation Problem

Since our goal is not only to show the differences between the equilibrium and kinetic carbonate models but also to demonstrate the necessity to iterate between the solute transport and chemical modules, we assume in this simulation that there is initially no calcite present in the soil profile.

We assume a 100-cm-deep soil profile with an initial pressure head of −500 cm. The hydraulic parameters of a hypothetical loam soil were derived from the retention curve given by *Hillel and van Bavel* [1976] (θ_r = 0.000, θ_s = 0.480, n = 1.592, α = 0.015022 cm^{-1}, and K_s = 60.48 cm d^{-1}). The upper boundary condition was an irrigation intensity of 1 cm d^{-1}, whereas the unit vertical hydraulic gradient [*McCord*, 1991] was utilized as the lower boundary condition. The potential root water uptake was distributed linearly throughout the whole soil profile with a maximum at the soil surface and zero uptake at the bottom of the root zone. The together with the irrigation intensity of 1 cm d^{-1} results in a

leaching fraction of 0.1. The water stress response function $a(h)$ was assumed to be equal to 1 for all pressure heads; i.e., there was no reduction of the potential root water uptake. Cauchy and Neumann boundary conditions were assumed at the surface and at the bottom of the soil profile, respectively. The bulk density of the soil was taken as 1.3 g cm^{-3} and molecular diffusion as 30 cm^2 d^{-1}. Both longitudinal and transverse dispersivities were equal to zero.

The solution composition of the irrigation water, as well as of the water initially present in the soil profile, is that of a calcite supersaturated well water from the Wellton-Mohawk Irrigation District (well 15: Ca_T = 12.2, Mg_T = 9.66, Na_T = 37.5, K_T = 0.27, Cl_T = 31.1, SO_{4T} = 19.5, and Alk = 6.5, all concentrations in millimoles charge per liter [*Suarez*, 1977]). The simulation was run at a temperature of 25°C. The soil CO_2 partial pressure was assumed to be equal to the atmospheric value at the soil surface (35 Pa) and to increase linearly with depth up to 2 kPa at the bottom of the soil profile. Cation exchange was not considered.

Figure 1 shows the water content profile at various times during the simulation. Due to the lower boundary condition (free drainage), the lower part of the soil profile is initially drained before the moisture front reaches these depths. A steady state profile is reached after approximately 150 days. The concentration profiles for the tracer, shown in Figure 2, indicate that the soil profile was initially free of tracer. The irrigation water had a tracer concentration of unity. The tracer becomes gradually more concentrated as it moves through the root zone due to evapotranspiration, reaching the steady state concentration of 10 at the bottom of the root zone, as expected for a leaching fraction of 0.1.

Figure 3 shows the Ca concentrations for the two different methods of coupling the solute transport part of the model with the chemical submodel, both assuming calcite equilibrium. In the first case there was no iteration process between the two modules and the chemical module was called after the solute transport module just to bring the solution to chemical equilibrium. A similar approach has been used in earlier models such as LEACHM [*Wagenet and Hutson*, 1987] and DYNAMIX [*Liu and Narasimhan*, 1989a, b]. In

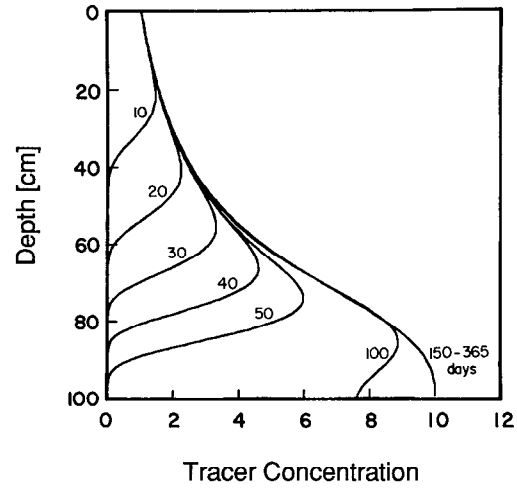

Figure 2. Tracer concentration profiles at various times after application with the irrigation water.

the second simulation we iterated between the chemistry and solute transport modules at each time step. The initial Ca concentration profile gradually increases from the surface to the bottom of the soil profile, as a result of the increase in CO_2 concentration with depth and corresponding increase in calcite solubility. The Ca concentrations increase with time due to two factors, enhanced solubility with increasing ionic strength and increasing Ca/alkalinity ratio as precipitation proceeds. Due to precipitation Ca increases only by a factor of three in contrast to the tenfold increase in the tracer concentration. Below the depth of 60 cm, the Ca concentrations are almost constant with depth due to precipitation of gypsum. Comparison of the simulations with and without iteration between modules shows that there are differences of about 1 $mmol_c$ L^{-1} Ca in the upper 50 cm of the soil profile. From Figure 3 it appears that the iteration process is not necessary, since the differences in Ca concentrations are

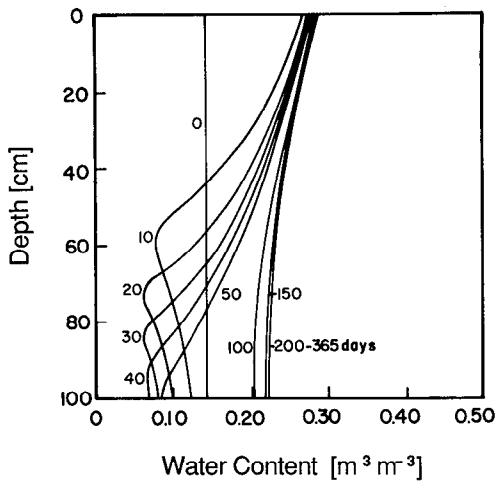

Figure 1. Soil water content profiles at various times after irrigation with saline drainage water (leaching fraction of

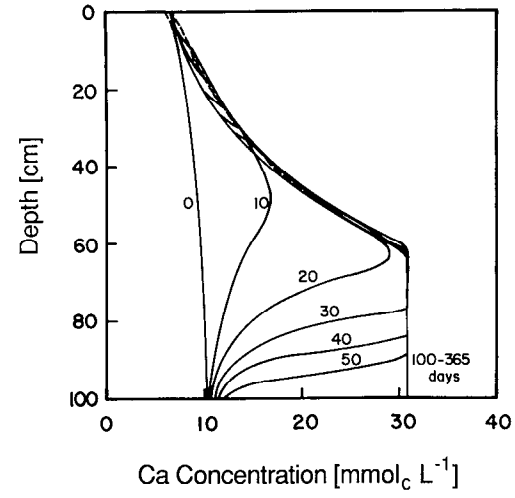

Figure 3. Calcium concentration profiles at various times considering instantaneous calcite precipitation/dissolution. Solid and dashed lines correspond to the cases with and and chemical modules, respectively.

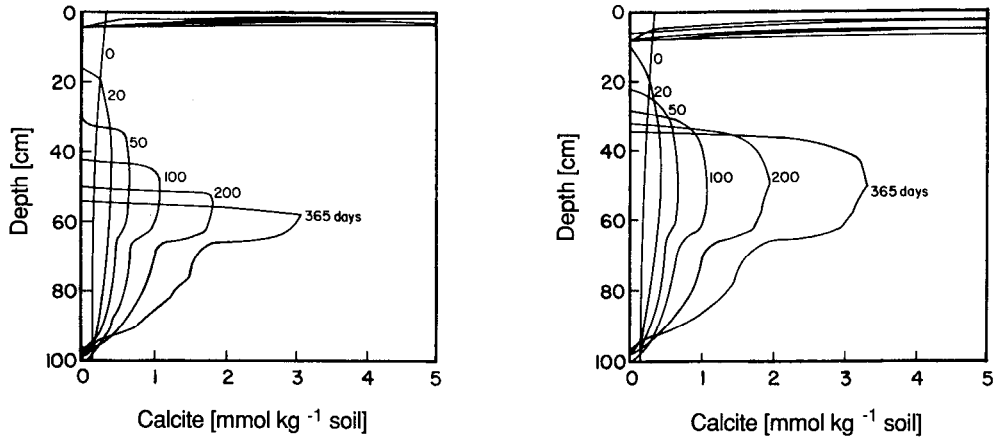

Figure 4. Calcite profiles at various times considering instantaneous precipitation/dissolution of calcite for the case (left) with and (right) without an iterative process between the solute transport and chemical modules.

almost negligible. However, even such small differences can have a large impact on precipitation of the solid phases, and especially on the position of their deposition. This is particularly important in paleoclimatic reconstructions which are based on depth to a caliche layer.

Figure 4 shows the distribution of calcite precipitation in the soil profile at different times, both with and without iterations between the modules. While in both cases there is a comparable amount of precipitated calcite in the whole soil profile throughout the simulation time (difference is less than 5%), there is a difference in the positions of the calcite precipitation zones. For the case without iteration a precipitation zone is simulated in the first four elements while for the case with iteration it is only within the first element. With iteration there is much more calcite precipitation at the soil surface and less within the soil profile than without iteration. Also, without iteration, the other main precipitation zone is between 35 and 65 cm, while with iteration this zone is much thinner and is located between about 55 and 65 cm. When calcite oversaturated irrigation water enters the soil profile the solution is immediately brought to equilibrium and while it moves to lower depths there are two opposing factors with respect to calcite saturation. Root water uptake concentrates the salts, thus increasing the tendency toward precipitation while increasing CO_2 with depth decreases this tendency. Figure 4 shows for both cases that immediately below the surface layer there is a zone of calcite dissolution followed by the zone of calcite precipitation. The position separating these two zones is moving downward with time and for the case without iterations lags significantly behind the front for the case with iterations. Below the 65-cm depth there is a significant decrease in calcite precipitation due to the competing effect of gypsum precipitation. The precise prediction of the position of precipitation zones is important, since it can have a significant effect on plant growth and formation of indurated layers.

The comparison of the gypsum precipitation with depth and time (not shown) indicated relatively small differences with and without iteration. The simulation with iteration has a better defined maxima in the precipitation front.

When calcite is precipitated throughout the whole soil profile (Figure 5), which is more realistic than the results shown on Figure 4. The calcite surface area was taken as 0.0005 m^2/dm^3 of soil. Again, as in Figure 4, there is a significant decrease in calcite precipitation below the 60 cm depth due to the concurrent precipitation of gypsum. Most of the calcite is precipitated close to the soil surface, but in a broader band when the kinetic model is used. There is also no area with calcite undersaturation in the soil profile. The pIAP values (pIAP is defined as the negative logarithm of the ion activity product, $-\log[(Ca^{2+})(CO_3^{2-})]$) simulated are in the range of 8.25–8.45 below the 25-cm depth, which is more than values typically found in arid zone soils [*Suarez*, 1985]. For purposes of demonstrating various aspects of the model, we considered simulations with steady boundary conditions which resulted in relatively gradual change in the values of particular variables. For transient boundary conditions with faster changes in, for example, water content and CO_2 concentration (which was not considered here), the range of pIAP values can be much higher (SS, 1994).

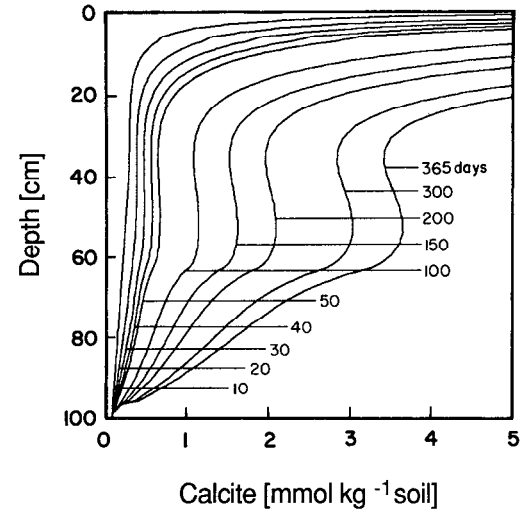

Effect precipitation/dissolution of calcite, considering ki

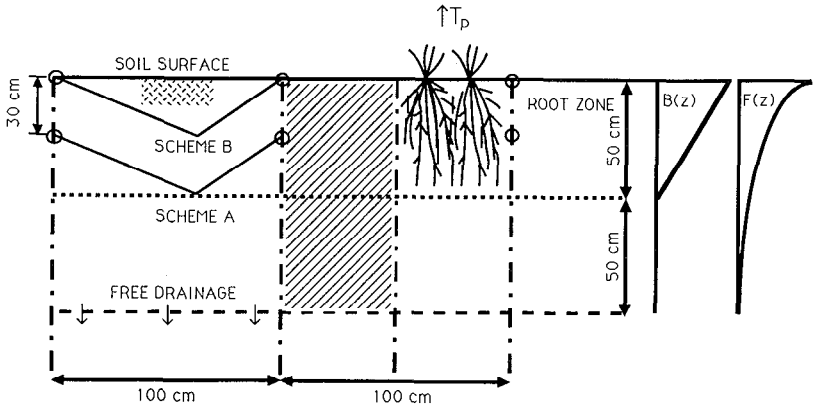

Figure 6. Schematic representation of the flow domain for the surface and subsurface line source irrigation systems.

4.2. Two-Dimensional Irrigation Problem

In this example we consider two different irrigation schemes (A and B). For the first irrigation scheme (scheme A) water is delivered into the soil profile by means of subsurface irrigation, for the second scheme (scheme B) surface drip irrigation is considered. The irrigation devices are assumed to be located 1 m apart and either 30 cm below the soil surface (A), or at the soil surface (B) (Figure 6). Because of the symmetry of the flow and transport fields, it is necessary to perform calculations only for the part of the profile between an irrigation device and the midpoint distance to the next device (lined area in Figure 6). The soil properties are the same as in the first example.

Potential root water uptake was distributed linearly throughout the soil profile with a maximum at the soil surface and zero uptake at and below the 50-cm depth. The total water uptake was taken as 0.4 cm d^{-1}. The water stress response function $a(h)$ used was that proposed by *Feddes et al.* [1978]. Water uptake is assumed to be zero close to saturation (i.e., wetter than some arbitrary "anaerobiosis point" h_1) and for $h < h_4$ (the wilting point pressure head). Water uptake is considered optimal between pressure heads h_2 and h_3, whereas for pressure heads between h_3 and h_4 (or h_1 and h_2), water uptake decreases (or increases) linearly with h. The following pressure head values were used to define the water stress response function $a(h)$: $h_1 = -25$ cm, $h_2 = -100$ cm, $h_3 = -275$ cm, and $h_4 = -8000$ cm.

The initial pressure head condition for both schemes was -200 cm. The unit vertical hydraulic gradient (free drainage) was used as the lower boundary condition and the rest of the boundary was assumed impermeable. The irrigation water was applied at the rate of 20 cm^2 d^{-1}, either 30 cm below the soil surface, through the node with the flux boundary condition (scheme A) or at the soil surface (scheme B), at the left side of the profile. In this example the applied irrigation is equal to the potential transpiration of the plant roots. Because of the reduction of the potential transpiration, a minimal amount of leaching did occur.

Figures 7 and 8 show the pressure head profiles for schemes A and B, respectively, at four different times. For scheme A there is a very dry region at and near the soil surface farthest away from the line source, where the pressure heads at the end of the simulation time are lower than -50 m. As a consequence of these pressure heads, root water uptake is significantly reduced and much less water flows into this region. A similar region also develops with surface irrigation, but the pressure heads do not reach such low values. Under surface irrigation the whole root zone is within the optimal range of pressure heads for plants for the entire simulation. For both schemes the bottom of the flow region becomes drier during the simulation due to the free

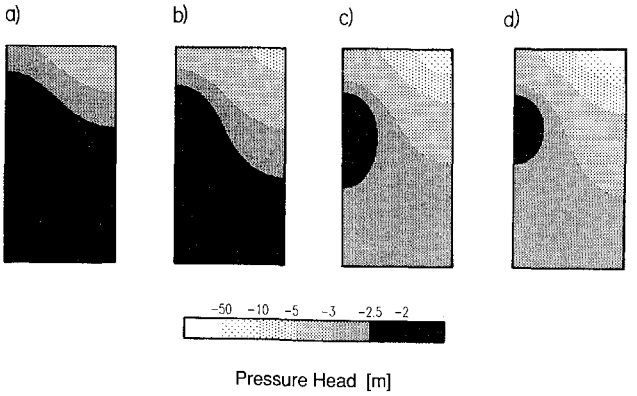

Figure 7. Pressure head profiles with subsurface irrigation (scheme A) at times (a) 10, (b) 25, (c) 50, and (d) 100 days.

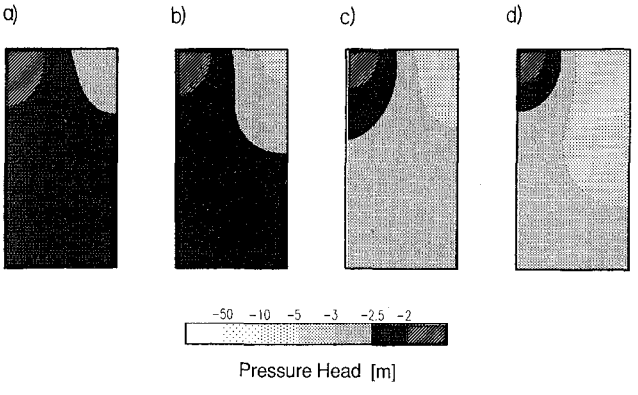

Figure 8. Pressure head profiles with surface irrigation (scheme B) at times (a) 10, (b) 25, (c) 50, and (d) 100 days.

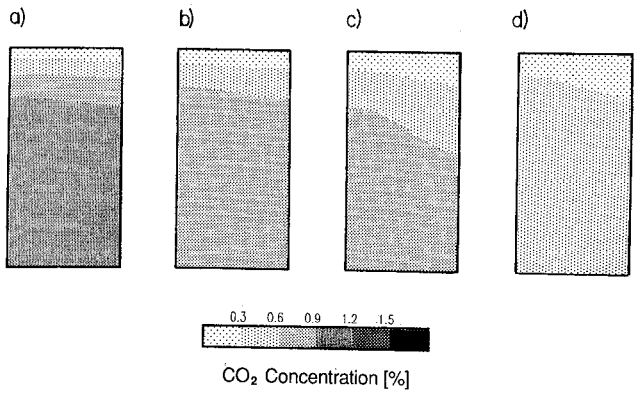

Figure 9. CO_2 profiles for scheme A at times (a) 10, (b) 25, (c) 50, and (d) 100 days.

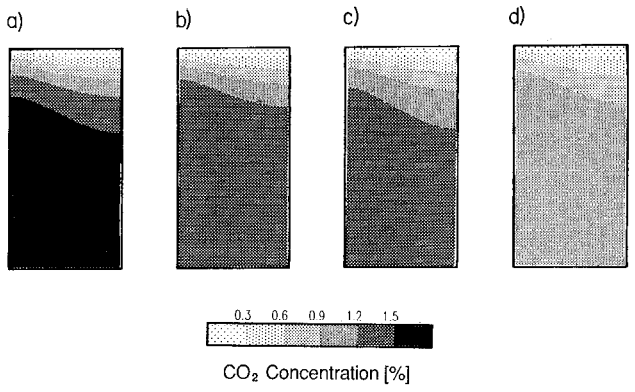

Figure 10. CO_2 profiles for scheme B at times (a) 10, (b) 25, (c) 50, and (d) 100 days.

drainage boundary conditions. At the end of the simulation the surface layer for scheme A is much drier than for scheme B, and that has significant consequences for both the CO_2 concentrations throughout the soil profile and the corresponding soil chemical reactions, such as calcite precipitation-dissolution.

For both schemes we simulated the CO_2 concentrations in the soil profile. We assumed that the optimal total CO_2 production rate (γ_0 = 0.007 m^3 m^{-2} d^{-1} [*Suarez and Šimůnek*, 1993]) is equal to the sum of the CO_2 production rate by plant roots and soil microorganisms and that plant roots account for 40% of the total CO_2 production. Further, we assumed that the spatial distribution of CO_2 root production corresponds to the spatial distribution of root water uptake and that CO_2 soil production is distributed exponentially within the soil profile [*Šimůnek and Suarez*, 1993]

$$f(z) = ae^{-a(z_0-z)}$$

where a is an empirical constant [L^{-1}] (=0.105 m^{-1} [*Suarez and Šimůnek*, 1993]), z_0 is the vertical coordinate of the soil surface [L] and $f(z)$ is the CO_2 production distribution coefficient. We considered that the optimal CO_2 production is reduced only due to the effect of the pressure head. We used the same reduction function for the CO_2 root production and root water uptake. Production of CO_2 in the profile is assumed to be zero at saturation; then it linearly increases until it reaches an optimal value at the pressure head h_1 (1 m) and further linearly decreases to zero at the pressure head h_2 (10^6 m). The scale for the pressure head–CO_2 production relationship is logarithmic [*Šimůnek and Suarez*, 1993]. The diffusion constants, and Henry's law constant were those used by *Suarez and Šimůnek* [1993]. We prescribed Neumann boundary conditions on all boundaries with the exception of the soil surface where CO_2 partial pressure was considered to be in equilibrium with the atmosphere (35 Pa). The initial CO_2 concentration condition for both schemes was 0.01 cm^3 cm^{-3}.

Figures 9 and 10 show CO_2 profiles for both schemes at four different times. For both schemes the CO_2 concentration increases at the beginning of the simulation when the moisture is uniformly distributed and then gradually decreases throughout the soil profile as the moisture is distributed. The CO_2 flux in the atmosphere at the upper right corner of the flow domain with lower water content. The decrease in CO_2 concentration is much faster with scheme A because the soil surface becomes much drier than for scheme B and thus causes faster CO_2 flux into the atmosphere. The amount of CO_2 in the soil profile at the end of the simulation for scheme B is almost the same as at the beginning, while for scheme A it is only about 60% of the initial value. Since the soil surface is relatively wetter with scheme B compared with scheme A, there are larger CO_2 gradients with scheme B near the soil surface.

The solution composition of the irrigation water, as well as of the water initially present in the soil profile is that of a calcite undersaturated Colorado river water from the Grand Valley (Ca_T = 2.63, Mg_T = 1.05, Na_T = 2.55, K_T = 0.06, Cl_T = 1.94, SO_{4T} = 2.03, and Alk = 2.33 $mmol_c$ L^{-1} [*Rhoades and Suarez*, 1977]). Cauchy and Neumann boundary conditions were assumed at the irrigation source and at the rest of the boundary, respectively. The same transport coefficients were used as in the first example. Cation exchange was not considered for these examples. The precipitation-dissolution of calcite was considered as a kinetic process with a calcite surface area of 0.0005 m^2/dm^3 of soil.

Figures 11 and 12 present the distribution of the hypothetical tracer for subsurface and surface irrigation schemes, respectively. The tracer is applied at unit concentration with the irrigation water into an initially tracer-free soil profile.

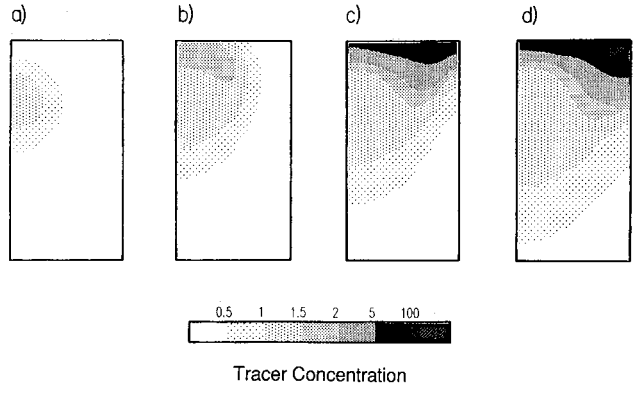

(b) 25, (c) 50, and (d) 100 days.

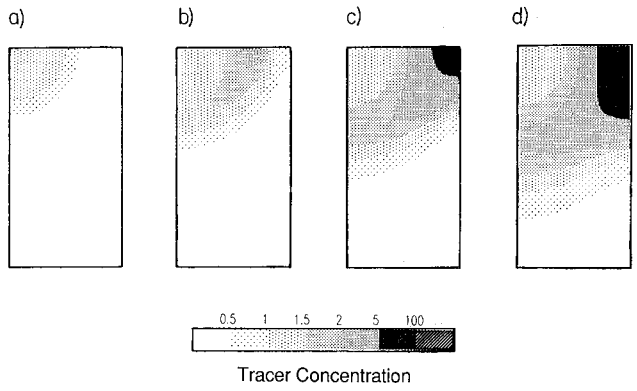

Figure 12. Tracer distribution for scheme B at times (a) 10, (b) 25, (c) 50, and (d) 100 days.

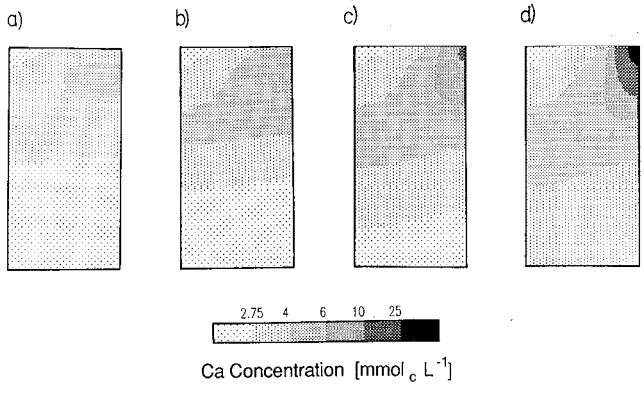

Figure 14. Calcium concentration for scheme B at times (a) 10, (b) 25, (c) 50, and (d) 100 days.

The infiltrating water immediately becomes more saline due to root water uptake. The tracer profiles are significantly different for schemes A and B. For scheme A the highest tracer concentrations are reached at the soil surface with extremes (values higher than 100) forming a band at the surface around the axis between the irrigation lines (top right corner of Figure 11). The maximum is not exactly at the surface because at the end of the simulation the pressure heads at that point reached such high values that root water uptake was completely suppressed, and the low hydraulic conductivity and high tortuosity factor essentially prevented further water or solute transport to this point. For scheme B the high tracer concentrations form a band which begins at the surface between the irrigation lines and ends at the bottom of the root zone below the irrigation source. The extremes in this case are located in the region between the irrigation sources and propagate slowly from the surface into deeper depths.

The Ca distribution for subsurface and surface irrigation schemes is presented in Figures 13 and 14, respectively, for four different times. At the end of the simulation the Ca profiles closely resemble those of the tracer, only the ratio between the Ca concentrations at the end to those at the beginning of the simulation are not as large because of calcite precipitation. Close to the surface between the irrigation lines (upper right corner) of scheme A, the extremes in tracer concentrations are not matched by maximums in Ca concentrations. This outcome is the result of decreasing calcite solubility once a critical ionic strength is reached when activity coefficients start to increase with increasing ionic strength. Therefore the Ca concentrations in equilibrium with calcite are lower here than in surrounding regions.

The distribution of precipitated calcite for both schemes is shown in Figures 15 and 16. For both schemes there is significant calcite precipitation directly at the soil surface due to the low CO_2 concentration in this region. For the first scheme the region of major calcite precipitation is concentrated in a band which extends from the soil surface to the depth which increases with the horizontal distance from the irrigation source. At the end of the simulation this band submerges in the middle between the irrigation sources. The reason for this is, as is discussed above for the tracer, the relative nonaccessibility of this surface layer for water and dissolved ions, due to the very low pressure heads and corresponding hydraulic conductivities. For surface irrigation, calcite precipitation begins similarly at the soil surface, but with time it is concentrated more in the middle between the irrigation sources. This precipitation region extends into intermediate depths below the irrigation source.

The profiles of pIAP for subsurface and surface irrigation schemes are presented in Figures 17 and 18, respectively. Initially both profiles are calcite undersaturated (pIAP >

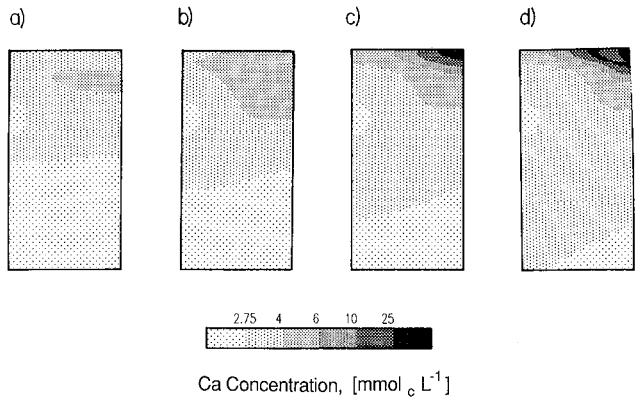

(a) 10, (b) 25, (c) 50, and (d) 100 days.

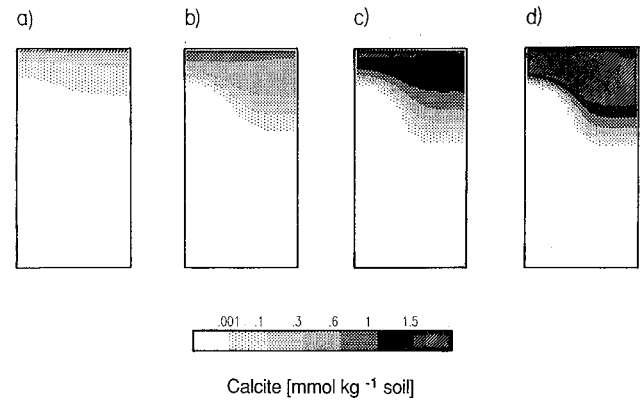

10 (b) 25, (c) 50, and (d) 100 days.

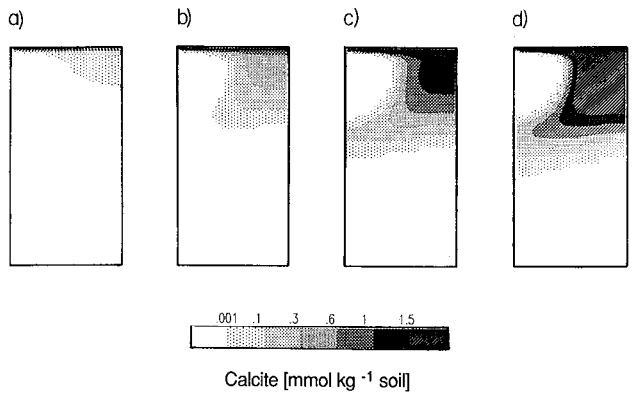

Figure 16. Distribution of calcite for scheme B at times (a) 10, (b) 25, (c) 50, and (d) 100 days.

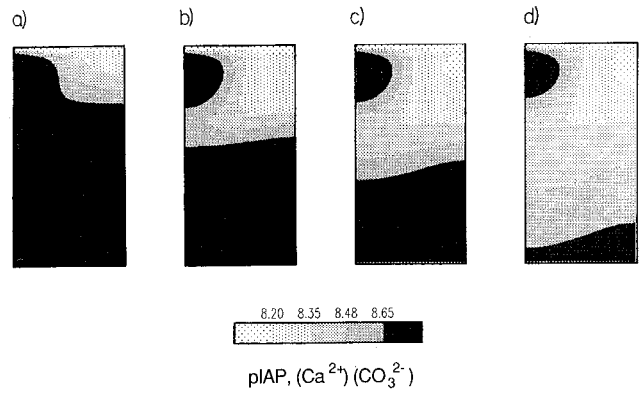

Figure 18. Calcite *p*IAP values for scheme B at times (a) 10, (b) 25, (c) 50, and (d) 100 days.

8.48). With time, as CO_2 concentrations in the upper layers decrease and the soil solution becomes more concentrated due to root water uptake, the soil solution becomes supersaturated and calcite is precipitated. At the end of the simulation most of the root zone is supersaturated with calcite. Although detailed field information on a two-dimensional problem such as this is not available, limited data [*Suarez*, 1983; D. L. Suarez, unpublished data, 1993], indicate that these simulations provide more realistic results than equilibrium simulations.

5. Discussion and Summary

The developed two-dimensional finite element model UNSATCHEM-2D is intended for modeling the major ion equilibrium and kinetic nonequilibrium chemistry in variably saturated porous media and is particularly useful for near Earth surface conditions where plant water uptake and CO_2 fluctuations must be considered. The model includes transient water movement in saturated-unsaturated porous media, multicomponent solute transport, heat transport, and carbon dioxide production and transport, as well as a chemical model that considers complexation reactions, cation exchange, and precipitation-dissolution reactions. All reactions apart from the precipitation-dissolution of calcite and dissolution of dolomite were considered as instantaneous. Precipitation-dissolution of calcite and dissolution of dolomite was modeled as either an equilibrium or multicomponent kinetic processes which includes both forward and back reactions. Both modified Debye-Hückel and Pitzer equations were incorporated into the model to calculate ion activities. By combining all these processes into a two dimensional model, UNSATCHEM-2D offers the possibility to more realistically simulate the complex chemical changes under field conditions both spatially and with time.

We demonstrated the model using two examples considering unsaturated transient water movement. The need for an iterative coupling procedure between the solute transport and chemical modules was demonstrated with a one-dimensional example with root water uptake and irrigation using moderately saline water. While the iteration process was necessary to predict correctly the precipitation zones and the total precipitated amount (see also *Yeh and Tripathi* [1991]), it seems that this time-consuming iteration process can be avoided if there is interest only in the aqueous concentrations. In the same example we also showed simulations with both equilibrium and kinetic controls on calcite precipitation. The utility of the model was further illustrated in two-dimensional simulations with surface and subsurface line irrigations. The results demonstrated the ability to simulate development of different solute concentration patterns and different spatial distribution of calcite precipitation with highly concentrated soil solution.

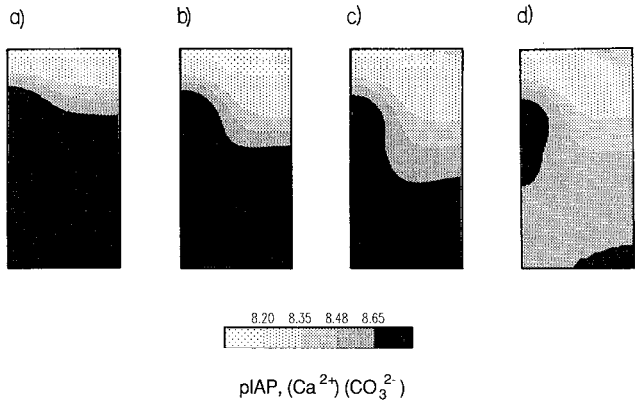

10, (b) 25, (c) 50, and (d) 100 days.

Appendix

The coefficients in (61) have the following form for cations, anions, and neutral species [*Felmy and Weare*, 1986]

$$\ln \gamma_M = z_M^2 F + \sum_a m_a (2B_{Ma} + ZC_{Ma}) + \sum_c m_c \left(2\Phi_{Mc} + \sum_a m_a \psi_{Mca}\right) + \sum_a \sum_{<a'} m_a m_{a'} \psi_{aa'M} + |z_M| \sum_c \sum_a m_c m_a C_{ca}$$

$$+ \sum_n \quad + \sum_n \sum_a \qquad (A1a)$$

$$\ln \gamma_X = z_X^2 F + \sum_c m_c(2B_{Xc} + ZC_{Xc}) + \sum_a m_a(2\Phi_{Xa} + \sum_c m_c\psi_{Xca}) + \sum_c \sum_{<c'} m_c m_{c'}\psi_{cc'X} + |z_X| \sum_c \sum_a m_c m_a C_{ca} + \sum_n m_n(2\lambda_{nX}) + \sum_n \sum_c m_n m_c \xi_{ncX} \quad \text{(A1b)}$$

$$\ln \gamma_N = \sum_c m_c(2\lambda_{Nc}) + \sum_a m_a(2\lambda_{Na}) + \sum_c \sum_a m_c m_a \xi_{Nca} \quad \text{(A1c)}$$

where z is the charge [dimensionless], m is the molality (moles per kilogram), subscripts M, X, N, and c, a, n refer to cations, anions, and neutrals, respectively, and where

$$F = -A^{\phi}\left(\frac{I^{1/2}}{1 + bI^{1/2}} + \frac{2}{b}\ln(1 + bI^{1/2})\right) + \sum_c \sum_a m_c m_a B'_{ca} + \sum_c \sum_{<c'} m_c m_{c'}\Phi'_{cc'} + \sum_a \sum_{<a'} m_a m_{a'}\Phi'_{aa'} \quad \text{(A2a)}$$

$$C_{MX} = \frac{C^{\phi}_{MX}}{2|Z_M Z_X|^{1/2}} \quad \text{(A2b)}$$

$$Z = \sum_i |z_i| m_i \quad \text{(A2c)}$$

and where A^{ϕ} is one third of the Debye-Hückel limiting slope and equal to 0.39 at 25°C.

The second virial coefficients B are given by the following ionic strength dependence [*Pitzer*, 1973]:

$$B^{\phi}_{MX} = \beta^{(0)}_{MX} + \beta^{(1)}_{MX} \exp(-\alpha_1\sqrt{I}) + \beta^{(2)}_{MX} \exp(-\alpha_2\sqrt{I}) \quad \text{(A3a)}$$

$$B_{MX} = \beta^{(0)}_{MX} + \beta^{(1)}_{MX} g(\alpha_1\sqrt{I}) + \beta^{(2)}_{MX} g(\alpha_2\sqrt{I}) \quad \text{(A3b)}$$

$$B'_{MX} = \beta^{(1)}_{MX}\frac{g'(\alpha_1\sqrt{I})}{I} + \beta^{(2)}_{MX}\frac{g'(\alpha_2\sqrt{I})}{I} \quad \text{(A3c)}$$

The functions g and g' are defined by

$$g(x) = 2\frac{(1 - (1 + x)e^{-x})}{x^2} \quad \text{(A4a)}$$

$$g'(x) = -2\frac{\left(1 - \left(1 + x + \frac{x^2}{2}\right)e^{-x}\right)}{x^2} \quad \text{(A4b)}$$

with $x = \alpha_1 I^{0.5}$ or $= \alpha_2 I^{0.5}$. When either cation M or anion X is univalent $\alpha_1 = 2$. For 2-2 or higher valence pairs, $\alpha_1 = 1.4$ and $\alpha_2 = 12$. The second virial coefficients Φ, which depend upon ionic strength, are in the form [*Pitzer*, 1973]

$$\Phi^{\Phi}_{ij} = \theta_{ij} + \theta^{E}_{ij}(I) + I\theta^{E'}_{ij}(I) \quad \text{(A5a)}$$

$$\Phi_{ij} = \theta_{ij} + \theta^{E}_{ij}(I) \quad \text{(A5b)}$$

$$\Phi'_{ij} = \theta^{E'}_{ij}(I) \quad \text{(A5c)}$$

The functions $\theta^{E}_{ij}(I)$ and $\theta^{E'}_{ij}(I)$ are a function only of ionic strength and the electrolyte pair type.

The second and third virial coefficients λ_{ni} and ξ_{nij}, representing the interactions between ions and neutral species, are assumed constant. The third virial coefficients C^{ϕ}_{MX} and ψ_{ijk} are also assumed to be independent of ionic strength.

References

Abriola, L. M., Modeling contaminant transport in the subsurface: An interdisciplinary challenge, *Rev. Geophys.*, *25*(2), 125–134, 1987.

Bear, J., *Dynamics of Fluid in Porous Media*, Elsevier, New York, 1972.

Bresler, E., Simultaneous transport of solute and water under transient unsaturated flow conditions, *Water Resour. Res.*, *9*, 975–986, 1973.

Bryant, S. L., R. S. Schechter, and L. W. Lake, Interactions of precipitation/dissolution waves and ion exchange in flow through permeable media, *AIChE J.*, *32*(5), 751–764, 1986.

Busenberg, E., and L. N. Plummer, The kinetics of dissolution of dolomite in CO_2-H_2O systems at 1.5 to 65 C and 0 to 1 ATM P_{CO_2}, *Am. J. Sci.*, *282*, 45–78, 1982.

Cederberg, G. A., R. L. Street, and J. O. Leckie, A groundwater mass transport and equilibrium chemistry model for multicomponent systems, *Water Resour. Res.*, *21*(8), 1095–1104, 1985.

Celia, M. A., and E. T. Bouloutas, and R. L. Zarba, A general mass-conservative numerical solution for the unsaturated flow equation, *Water Resour. Res.*, *26*(7), 1483–1496, 1990.

de Jong, E., and H. Schappert, Calculation of soil respiration and activity from CO_2 profiles in the soil, *Soil Sci.*, *113*(5), 328–333, 1972.

Dudley, L. M., R. J. Wagenet, and J. J. Jurinak, Description of soil chemistry during transient solute transport, *Water Resour. Res.*, *17*(5), 1498–1504, 1981.

Feddes, R. A., P. J. Kowalik, and H. Zaradny, *Simulation of Field Water Use and Crop Yield, Simulation Monographs*, Pudoc, Wageningen, The Netherlands, 1978.

Felmy, A. R., and J. H. Weare, The prediction of borate mineral equilibria in natural waters: Application to Searles Lake, California, *Geochim. Cosmochim. Acta*, *50*, 2771–2783, 1986.

Förster, R., A multicomponent transport model, *Geoderma*, *38*, 261–278, 1986.

Förster, R., and H. Gerke, Integration von Modellen des Wasser- und Stofftransports sowie physikochemischer Wechselwirkungen zur Analyse von Agrar-Ökosystemen, in *Verhandlungen der Gesellschaft für Ökologie*, Band XVIII, pp. 515–522, University of Göttingen, Göttingen, Germany, 1989.

Glinski, J., and W. Stepniewski, *Soil Aeration and Its Role for Plants*, CRC Press, Boca Raton, Fl., 1985.

Gureghian, A. B., A two-dimensional finite-element solution for the simultaneous transport of water and multisolutes through a nonhomogeneous aquifer under transient saturated-unsaturated flow conditions, *Sci. Total Environ.*, *21*, 329–337, 1981.

Harvie, Ch. E., N. Moller, and J. H. Weare, The prediction of mineral solubilities in natural waters: The Na-K-Mg-Ca-H-Cl-SO_4-OH-HCO_3-CO_3-H_2O-system to high ionic strengths at 25°C, *Geochim. Cosmochim. Acta*, *48*, 723–751, 1984.

Hillel, D., and C. H. M. van Bavel, Simulation of profile water storage as related to soil hydrologic properties, *Soil Sci. Soc. Am. J.*, *40*, 807–815, 1976.

Huyakorn, P. S., and G. F. Pinder, *Computational Methods in Subsurface Flow*, Academic, San Diego, Calif., 1983.

Huyakorn, P. S., S. D. Thomas, and B. M. Thompson, Techniques for making finite elements competitive in modeling flow in variably saturated porous media, *Water Resour. Res.*, *20*(8), 1099–1115, 1984.

Huyakorn, P. S., P. F. Andersen, J. W. Mercer, and H. O. White, Saturated-unsaturated porous media flow simulation with mass transport, *Water Resour. Res.*, *23*(2), 293–312, 1987.

Kirkham, D., and W. L. Powers, *Advanced Soil Physics*, Wiley-Interscience, New York, 1972.

Kool, J. B., and J. C. Parker, Development and evaluation of closed-form expressions for hysteretic soil hydraulic properties, *Water Resour. Res.*, *23*(1), 105–114, 1987.

Kool, J. B., J. C. Parker, and M. Th. van Genuchten, Parameter estimation for unsaturated flow and transport models—A review, *J. Hydrol.*, *91*, 255–293, 1987.

Kool, J. B., J. C. Parker, and M. Th. van Genuchten, Determining soil hydraulic properties from one-step outflow experiments by parameter estimation: I. Theory and numerical studies, *Soil Sci. Soc. Am. J.*, *49*, 1348–1354, 1985.

Lichtner, P. C., Continuum model for simultaneous chemical reactions and mass transport in hydrothermal systems, *Geochim. Cosmochim. Acta*, *49*, 779–800, 1985.

Lichtner, P. C., Continuum formulation of multicomponent-multiphase reactive transport, in *Reactive Transport in Porous Media*, *Rev. Mineral.*, *34*, edited by P. C. Lichtner, C. I. Steefel, and E. H. Oelkers, pp. 1–81, Mineralogical Society of America, Washington, D.C., 1996.

Mualem, Y., A new model for predicting the hydraulic conductivity of unsaturated porous media, *Water Resour. Res.*, *12*(3), 513–522, 1976.

Narasimhan, T. N., and P. A. Witherspoon, An integrated finite difference method for analyzing fluid flow in porous media, *Water Resour. Res.*, *12*(1), 57–64, 1976.

Neuman, S. P., Saturated-unsaturated seepage by finite elements, *J. Hydraul. Div. Am. Soc. Civ. Eng.*, *99*(HY12), 2233–2250, 1973.

Neuman, S. P., Adaptive Eulerian-Lagrangian finite element method for advection-dispersion, *Int. J. Numer. Methods Eng.*, *20*, 321–337, 1984.

Neuman, S. P., Universal scaling of hydraulic conductivities and dispersivities in geologic media, *Water Resour. Res.*, *26*(8), 1749–1758, 1990.

Parkhurst, D. L., D. C. Thorstenson, and L. N. Plummer, PHREEQE—A computer program for geochemical calculations, *U.S. Geol. Surv. Water Resour. Invest. Rep.*, *80-96*, 1980.

Pitzer, K. S., Thermodynamics of electrolytes: I. Theoretical basis and general equations, *J. Phys. Chem.*, *77*(2), 268–277, 1973.

Pitzer, K. S., Theory: Ion interaction approach, in *Activity Coefficients in Electrolyte Solutions*, edited by K. S. Pitzer, pp. 157–208, CRC Press, Boca Raton, Fl., 1991.

Pitzer, K. S., and G. Mayorga, Thermodynamics of electrolytes: II. Activity and osmotic coefficients for strong electrolytes with one or both ions univalent, *J. Phys. Chem.*, *77*(19), 2300–2308, 1973.

Pitzer, K. S., and G. Mayorga, Thermodynamics of electrolytes: III. Activity and osmotic coefficients for 2-2 electrolytes, *J. Solution Chem.*, *3*(7), 539–546, 1974.

Pitzer, K. S., and J. M. Simonson, Thermodynamics of multicomponent, miscible, ionic systems: Theory and equations, *J. Phys. Chem.*, *90*, 3005–3009, 1986.

Rubin, J., Transport of reacting solutes in porous media: Relation between mathematical nature of problem formulation and chemical nature of reactions, *Water Resour. Res.*, *19*(5), 1231–1252, 1983.

Šimůnek, J., and M. Th. van Genuchten, Modeling nonequilibrium flow and transport with HYDRUS, *Res. Rep. 129*, U.S. Salinity Lab., Riverside, Calif., 1994.

Šimůnek, J., and M. Th. van Genuchten, Modeling nonequilibrium flow and transport with HYDRUS, *Phys. Chem. Earth*, *21*(5–6), 317–322, 1996.

Šimůnek, J., and M. Th. van Genuchten, Modeling nonequilibrium flow and transport with HYDRUS, *J. Contam. Hydrol.*, *31*(3–4), 282–297, 1997.

Šimůnek, J., and M. Th. van Genuchten, Modeling nonequilibrium flow and transport with HYDRUS, *Res. Rep. 139*, U.S. Salinity Lab., Riverside, Calif., 1997.

Šimůnek, J., and M. Th. van Genuchten, Modeling nonequilibrium flow and transport with HYDRUS, *Res. Rep. 140*, U.S. Salinity Lab., Riverside, Calif., 1998.

Šimůnek, J., and M. Th. van Genuchten, Modeling nonequilibrium flow and transport with HYDRUS, *Res. Rep. 141*, U.S. Salinity Lab., Riverside, Calif., 1998.

Šimůnek, J., and M. Th. van Genuchten, Modeling nonequilibrium flow and transport with HYDRUS, *Res. Rep. 142*, U.S. Salinity Lab., Riverside, Calif., 1998.

Šimůnek, J., and M. Th. van Genuchten, Modeling nonequilibrium flow and transport with HYDRUS, *Res. Rep. 143*, U.S. Salinity Lab., Riverside, Calif., 1998.

Šimůnek, J., and M. Th. van Genuchten, Modeling nonequilibrium flow and transport with HYDRUS, *Res. Rep. 144*, U.S. Salinity Lab., Riverside, Calif., 1998.

Šimůnek, J., and M. Th. van Genuchten, Modeling nonequilibrium flow and transport with HYDRUS, *Res. Rep. 145*, U.S. Salinity Lab., Riverside, Calif., 1998.

Šimůnek, J., and M. Th. van Genuchten, Modeling nonequilibrium flow and transport with HYDRUS, *Res. Rep. 146*, U.S. Salinity Lab., Riverside, Calif., 1998.

Šimůnek, J., and M. Th. van Genuchten, Modeling nonequilibrium flow and transport with HYDRUS, *Res. Rep. 147*, U.S. Salinity Lab., Riverside, Calif., 1998.

Šimůnek, J., and M. Th. van Genuchten, Modeling nonequilibrium flow and transport with HYDRUS, *Res. Rep. 148*, U.S. Salinity Lab., Riverside, Calif., 1998.

Šimůnek, J., and M. Th. van Genuchten, Modeling nonequilibrium flow and transport with HYDRUS, *Res. Rep. 149*, U.S. Salinity Lab., Riverside, Calif., 1998.

Šimůnek, J., and M. Th. van Genuchten, Modeling nonequilibrium flow and transport with HYDRUS, *Res. Rep. 150*, U.S. Salinity Lab., Riverside, Calif., 1998.

Šimůnek, J., and M. Th. van Genuchten, Modeling nonequilibrium flow and transport with HYDRUS, *Res. Rep. 151*, U.S. Salinity Lab., Riverside, Calif., 1998.

Šimůnek, J., and M. Th. van Genuchten, Modeling nonequilibrium flow and transport with HYDRUS, *Res. Rep. 152*, U.S. Salinity Lab., Riverside, Calif., 1998.

Šimůnek, J., and M. Th. van Genuchten, Modeling nonequilibrium flow and transport with HYDRUS, *Res. Rep. 153*, U.S. Salinity Lab., Riverside, Calif., 1998.

Šimůnek, J., and M. Th. van Genuchten, Modeling nonequilibrium flow and transport with HYDRUS, *Res. Rep. 154*, U.S. Salinity Lab., Riverside, Calif., 1998.

Šimůnek, J., and M. Th. van Genuchten, Modeling nonequilibrium flow and transport with HYDRUS, *Res. Rep. 155*, U.S. Salinity Lab., Riverside, Calif., 1998.

Šimůnek, J., and M. Th. van Genuchten, Modeling nonequilibrium flow and transport with HYDRUS, *Res. Rep. 156*, U.S. Salinity Lab., Riverside, Calif., 1998.

Šimůnek, J., and M. Th. van Genuchten, Modeling nonequilibrium flow and transport with HYDRUS, *Res. Rep. 157*, U.S. Salinity Lab., Riverside, Calif., 1998.

Šimůnek, J., and M. Th. van Genuchten, Modeling nonequilibrium flow and transport with HYDRUS, *Res. Rep. 158*, U.S. Salinity Lab., Riverside, Calif., 1998.

Šimůnek, J., and M. Th. van Genuchten, Modeling nonequilibrium flow and transport with HYDRUS, *Res. Rep. 159*, U.S. Salinity Lab., Riverside, Calif., 1998.

Šimůnek, J., and M. Th. van Genuchten, Modeling nonequilibrium flow and transport with HYDRUS, *Res. Rep. 160*, U.S. Salinity Lab., Riverside, Calif., 1998.

Šimůnek, J., and M. Th. van Genuchten, Modeling nonequilibrium flow and transport with HYDRUS, *Res. Rep. 161*, U.S. Salinity Lab., Riverside, Calif., 1998.

Šimůnek, J., and M. Th. van Genuchten, Modeling nonequilibrium flow and transport with HYDRUS, *Res. Rep. 162*, U.S. Salinity Lab., Riverside, Calif., 1998.

Šimůnek, J., and M. Th. van Genuchten, Modeling nonequilibrium flow and transport with HYDRUS, *Res. Rep. 163*, U.S. Salinity Lab., Riverside, Calif., 1998.

Šimůnek, J., and M. Th. van Genuchten, Modeling nonequilibrium flow and transport with HYDRUS, *Res. Rep. 164*, U.S. Salinity Lab., Riverside, Calif., 1998.

Šimůnek, J., and M. Th. van Genuchten, Modeling nonequilibrium flow and transport with HYDRUS, *Res. Rep. 165*, U.S. Salinity Lab., Riverside, Calif., 1998.

Šimůnek, J., and M. Th. van Genuchten, Modeling nonequilibrium flow and transport with HYDRUS, *Res. Rep. 166*, U.S. Salinity Lab., Riverside, Calif., 1998.

Šimůnek, J., and M. Th. van Genuchten, Modeling nonequilibrium flow and transport with HYDRUS, *Res. Rep. 167*, U.S. Salinity Lab., Riverside, Calif., 1998.

Šimůnek, J., and M. Th. van Genuchten, Modeling nonequilibrium flow and transport with HYDRUS, *Res. Rep. 168*, U.S. Salinity Lab., Riverside, Calif., 1998.

Šimůnek, J., and M. Th. van Genuchten, Modeling nonequilibrium flow and transport with HYDRUS, *Res. Rep. 169*, U.S. Salinity Lab., Riverside, Calif., 1998.

Šimůnek, J., and M. Th. van Genuchten, Modeling nonequilibrium flow and transport with HYDRUS, *Res. Rep. 170*, U.S. Salinity Lab., Riverside, Calif., 1998.

Šimůnek, J., and M. Th. van Genuchten, Modeling nonequilibrium flow and transport with HYDRUS, *Res. Rep. 171*, U.S. Salinity Lab., Riverside, Calif., 1998.

Šimůnek, J., and M. Th. van Genuchten, Modeling nonequilibrium flow and transport with HYDRUS, *Res. Rep. 172*, U.S. Salinity Lab., Riverside, Calif., 1998.

Šimůnek, J., and M. Th. van Genuchten, Modeling nonequilibrium flow and transport with HYDRUS, *Res. Rep. 173*, U.S. Salinity Lab., Riverside, Calif., 1998.

Šimůnek, J., and M. Th. van Genuchten, Modeling nonequilibrium flow and transport with HYDRUS, *Res. Rep. 174*, U.S. Salinity Lab., Riverside, Calif., 1998.

Šimůnek, J., and M. Th. van Genuchten, Modeling nonequilibrium flow and transport with HYDRUS, *Res. Rep. 175*, U.S. Salinity Lab., Riverside, Calif., 1998.

Šimůnek, J., and M. Th. van Genuchten, Modeling nonequilibrium flow and transport with HYDRUS, *Res. Rep. 176*, U.S. Salinity Lab., Riverside, Calif., 1998.

Šimůnek, J., and M. Th. van Genuchten, Modeling nonequilibrium flow and transport with HYDRUS, *Res. Rep. 177*, U.S. Salinity Lab., Riverside, Calif., 1998.

Šimůnek, J., and M. Th. van Genuchten, Modeling nonequilibrium flow and transport with HYDRUS, *Res. Rep. 178*, U.S. Salinity Lab., Riverside, Calif., 1998.

Šimůnek, J., and M. Th. van Genuchten, Modeling nonequilibrium flow and transport with HYDRUS, *Res. Rep. 179*, U.S. Salinity Lab., Riverside, Calif., 1998.

Šimůnek, J., and M. Th. van Genuchten, Modeling nonequilibrium flow and transport with HYDRUS, *Res. Rep. 180*, U.S. Salinity Lab., Riverside, Calif., 1998.

Šimůnek, J., and M. Th. van Genuchten, Modeling nonequilibrium flow and transport with HYDRUS, *Res. Rep. 181*, U.S. Salinity Lab., Riverside, Calif., 1998.

Šimůnek, J., and M. Th. van Genuchten, Modeling nonequilibrium flow and transport with HYDRUS, *Res. Rep. 182*, U.S. Salinity Lab., Riverside, Calif., 1998.

Šimůnek, J., and M. Th. van Genuchten, Modeling nonequilibrium flow and transport with HYDRUS, *Res. Rep. 183*, U.S. Salinity Lab., Riverside, Calif., 1998.

Šimůnek, J., and M. Th. van Genuchten, Modeling nonequilibrium flow and transport with HYDRUS, *Res. Rep. 184*, U.S. Salinity Lab., Riverside, Calif., 1998.

Šimůnek, J., and M. Th. van Genuchten, Modeling nonequilibrium flow and transport with HYDRUS, *Res. Rep. 185*, U.S. Salinity Lab., Riverside, Calif., 1998.

Šimůnek, J., and M. Th. van Genuchten, Modeling nonequilibrium flow and transport with HYDRUS, *Res. Rep. 186*, U.S. Salinity Lab., Riverside, Calif., 1998.

Šimůnek, J., and M. Th. van Genuchten, Modeling nonequilibrium flow and transport with HYDRUS, *Res. Rep. 187*, U.S. Salinity Lab., Riverside, Calif., 1998.

Šimůnek, J., and M. Th. van Genuchten, Modeling nonequilibrium flow and transport with HYDRUS, *Res. Rep. 188*, U.S. Salinity Lab., Riverside, Calif., 1998.

Šimůnek, J., and M. Th. van Genuchten, Modeling nonequilibrium flow and transport with HYDRUS, *Res. Rep. 189*, U.S. Salinity Lab., Riverside, Calif., 1998.

Šimůnek, J., and M. Th. van Genuchten, Modeling nonequilibrium flow and transport with HYDRUS, *Res. Rep. 190*, U.S. Salinity Lab., Riverside, Calif., 1998.

Šimůnek, J., and M. Th. van Genuchten, Modeling nonequilibrium flow and transport with HYDRUS, *Res. Rep. 191*, U.S. Salinity Lab., Riverside, Calif., 1998.

Šimůnek, J., and M. Th. van Genuchten, Modeling nonequilibrium flow and transport with HYDRUS, *Res. Rep. 192*, U.S. Salinity Lab., Riverside, Calif., 1998.

Šimůnek, J., and M. Th. van Genuchten, Modeling nonequilibrium flow and transport with HYDRUS, *Res. Rep. 193*, U.S. Salinity Lab., Riverside, Calif., 1998.

Šimůnek, J., and M. Th. van Genuchten, Modeling nonequilibrium flow and transport with HYDRUS, *Res. Rep. 194*, U.S. Salinity Lab., Riverside, Calif., 1998.

Šimůnek, J., and M. Th. van Genuchten, Modeling nonequilibrium flow and transport with HYDRUS, *Res. Rep. 195*, U.S. Salinity Lab., Riverside, Calif., 1998.

Šimůnek, J., and M. Th. van Genuchten, Modeling nonequilibrium flow and transport with HYDRUS, *Res. Rep. 196*, U.S. Salinity Lab., Riverside, Calif., 1998.

Šimůnek, J., and M. Th. van Genuchten, Modeling nonequilibrium flow and transport with HYDRUS, *Res. Rep. 197*, U.S. Salinity Lab., Riverside, Calif., 1998.

Šimůnek, J., and M. Th. van Genuchten, Modeling nonequilibrium flow and transport with HYDRUS, *Res. Rep. 198*, U.S. Salinity Lab., Riverside, Calif., 1998.

Šimůnek, J., and M. Th. van Genuchten, Modeling nonequilibrium flow and transport with HYDRUS, *Res. Rep. 199*, U.S. Salinity Lab., Riverside, Calif., 1998.

Šimůnek, J., and M. Th. van Genuchten, Modeling nonequilibrium flow and transport with HYDRUS, *Res. Rep. 200*, U.S. Salinity Lab., Riverside, Calif., 1998.

variably saturated porous media, *Water Resour. Res.*, *21*(3), 346–358, 1985.

Huyakorn, P. S., J. B. Kool, and Y. S. Wu, VAM2D—Variably saturated analysis model in two dimensions, Version 5.2 with hysteresis and chained decay transport, Documentation and user's guide, *NUREG/CR-5352, Rev. 1*, U.S. Nucl. Reg. Comm., Washington, D.C., 1991.

Inskeep, W. P., and P. R. Bloom, An evaluation of rate equations for calcite precipitation kinetics at pCO_2 less than 0.01 atm and pH greater than 8, *Geochim. Cosmochim. Acta*, *49*, 2165–2180, 1985.

Inskeep, W. P., and P. R. Bloom, Kinetics of calcite precipitation in the presence of water-soluble organic ligands, *Soil Sci. Soc. Am. J.*, *50*, 1167–1172, 1986.

Jennings, A. A., D. J. Kirkner, and T. L. Theis, Multicomponent equilibrium chemistry in groundwater quality models, *Water Resour. Res.*, *18*(4), 1089–1096, 1982.

Kirkner, D. J., and H. Reeves, Multicomponent mass transport with homogeneous and heterogenous chemical reactions: Effect of the chemistry on the choice of numerical algorithm, 1, Theory, *Water Resour. Res.*, *24*(10), 1719–1729, 1988.

Kirkner, D. J., A. A. Jennings, and T. L. Theis, Multisolute mass transport with chemical interaction kinetics, *J. Hydrol.*, *76*, 107–117, 1985.

Lasaga, A. C., The treatment of multi-component diffusion and ion pairs in diagenetic fluxes, *Am. J. Sci.*, *279*, 324–346, 1979.

Liu, C.-W., and T. N. Narasimhan, Redox-controlled multiple-species reactive chemical transport, 1, Model development, *Water Resour. Res.*, *25*(5), 869–882, 1989a.

Liu, C.-W., and T. N. Narasimhan, Redox-controlled multiple-species reactive chemical transport, 2, Verification and application, *Water Resour. Res.*, *25*(5), 883–910, 1989b.

Mangold, D. C., and C.-F. Tsang, A summary of subsurface hydrological and hydrochemical models, *Rev. Geophys.*, *29*(1), 51–79, 1991.

McCord, J. T., Application of second-type boundaries in unsaturated flow modeling, *Water Resour. Res.*, *27*(12), 3257–3260, 1991.

Millington, R. J., and J. M. Quirk, Permeability of porous solids, *Trans. Faraday Soc.*, *57*, 1200–1207, 1961.

Mualem, Y., A new model for predicting the hydraulic conductivity of unsaturated porous media, *Water Resour. Res.*, *12*(3), 513–522, 1976.

Narasimhan, T. N., A. F. White, and T. Tokunaga, Groundwater contamination from an inactive uranium mill tailings pile, 2, Application of a dynamic mixing model, *Water Resour. Res.*, *22*(13), 1820–1834, 1986.

Neuman, S. P., Galerkin approach to saturated-unsaturated flow in porous media, *Finite Elements in Fluids*, vol. 1, *Viscous Flow and Hydrodynamics*, edited by R. H. Gallagher, J. T. Oden, C. Taylor, and O. C. Zienkiewicz, pp. 201–217, John Wiley, New York, 1975.

Neuman, S. P., R. A. Feddes, and E. Bresler, Finite element simulation of flow in saturated-unsaturated soils considering water uptake by plants, in *Third Annual Report, Proj. A10-SWC-77*, Hydraul. Eng. Lab., Technion, Haifa, Israel, 1974.

Patwardhan, A. S., J. L. Nieber, and I. D. Moore, Oxygen, carbon dioxide, and water transfer in soils: Mechanism and crop response, *Trans. ASEA*, *31*(5), 1383–1395, 1988.

Pinder, G. F., W. G. Gray, *Finite Element Simulation in Surface and Subsurface Hydrology*, Academic, San Diego, Calif., 1977.

Pitzer, K. S., Thermodynamics of electrolytes, I, Theoretical basis and general equations, *J. Phys. Chem.*, *77*, 268–277, 1973.

Pitzer, K. S., *Activity Coefficients in Electrolyte Solutions*, chap. 7, CRC Press, Boca Raton, Fla., 1979.

Plummer, L. N., T. M. Wigley, and D. L. Parkhurst, The kinetics of calcite dissolution in CO_2 systems at 5° to 60°C and 0.0 to 1.0 atm CO_2, *Am. J. Sci.*, *278*, 179–216, 1978.

Rhoades, J. D., and D. L. Suarez, Reducing water quality degradation through minimized leaching management, *Agric. Water Manage.*, *1*(2), 127–142, 1977.

Robbins, C. W., R. J. Wagenet, and J. J. Jurinak, A combined salt transport-chemical equilibrium model for calcareous and gypsiferous soils, *Soil Sci. Soc. Am. J.*, *44*, 1191–1194, 1980a.

Robbins, C. W., R. J. Wagenet, and J. J. Jurinak, Calculating cation exchange in a salt transport model, *Soil Sci. Soc. Am. J.*, *44*, [illegible] transport with multisegment, equilibrium controlled reactions: A feed forward simulation method, *Water Resour. Res.*, *26*(9), 2029–2055, 1990.

Russo, D., Simulation of leaching of a gypsiferous-sodic desert soil, *Water Resour. Res.*, *22*(8), 1341–1349, 1986.

Šimůnek, J., and D. L. Suarez, Modeling of carbon dioxide transport and production in soil, 1, Model development, *Water Resour. Res.*, *29*(2), 487–497, 1993.

Šimůnek, J., and D. L. Suarez, The UNSATCHEM-2D code for simulating two-dimensional variably saturated water flow, heat transport, carbon dioxide transport, and solute transport with major ion equilibrium and kinetic chemistry, Version 1.1, *Res. Rep. 128*, U.S. Salinity Lab. Agric. Res. Serv., U.S. Dept. of Agric., Riverside, Calif., 1994.

Šimůnek, J., and M. T. van Genuchten, The CHAIN-2D code for simulating two-dimensional movement of water, heat and multiple solutes in variably-saturated soils, *Agron. Abs.*, 217, 1993.

Šimůnek, J., T. Vogel, and M. T. van Genuchten, The SWMS-2D code for simulating water flow and solute transport in two-dimensional variably saturated media, Version 1.1, *Res. Rep. 126*, U.S. Salinity Lab., Agric. Res. Serv., U.S. Dept. of Agric., Riverside Calif., 1992.

Solomon, D. K., and T. E. Cerling, The annual carbon dioxide cycle in a Montane soil: Observation, modeling, and implication for weathering, *Water Resour. Res.*, *23*(12), 2257–2265, 1987.

Stokes, R. H., Thermodynamics of solutions, in *Activity Coefficients in Electrolyte Solutions*, edited by R. M. Pitkowicz, CRC Press, Boca Raton, Fl., 1979.

Suarez, D. L., Ion activity products of calcium carbonate in waters below the root zone, *Soil Sci. Soc. Am. J.*, *41*, 310–315, 1977.

Suarez, D. L., Prediction of major ion concentrations in arid land soils using equilibrium and kinetic theories, in ARS Modeling Symposium, *Rep. USDA-ARS-30*, pp. 170–175, Pingree Park, Colo., 1983.

Suarez, D. L., and J. Šimůnek, Modeling of carbon dioxide transport and production in soil, 2, parameter selection, sensitivity analysis and comparison of model predictions to field data, *Water Resour. Res.*, *29*(2), 499–513, 1993.

Suarez, D. L., and J. D. Rhoades, The apparent solubility of calcium carbonate in soils, *Soil Sci. Soc. Am. J.*, *46*, 716–722, 1982.

Truesdell, A. H., and B. F. Jones, Wateq, a computer program for calculating chemical equilibria of natural waters, *J. Res. U.S. Geol. Surv.*, *2*(2), 233–248, 1974.

Valocchi, A. J., R. L. Street, and P. V. Roberts, Transport of ion-exchanging solutes in groundwater: Chromatographic theory and field simulation, *Water Resour. Res.*, *17*(5), 1517–1527, 1981.

van Bavel, C. H. M., A soil aeration theory based on diffusion, *Soil Sci.*, *72*, 33–46, 1951.

van Genuchten, M. T., A closed-form equation for predicting the hydraulic conductivity of unsaturated soils, *Soil Sci. Soc. Am. J.*, *44*(5), 892–898, 1980.

Vogel, T., SWMII—Numerical model of two-dimensional flow in a variably saturated porous medium, *Res. Rep. 87*, Dept. of Hydraul. and Catchment Hydrol., Agric. Univ., Wageningen, The Netherlands, 1987.

Wagenet, R. J., and J. L. Hutson, LEACHM: *L*eaching *E*stimation *A*nd *CH*emistry *M*odel, A process-based model of water and solute movement, transformations, plant uptake and chemical reactions in the unsaturated zone, *Continuum 2*, Water Resour. Inst., Cornell Univ., Ithaca, N. Y., 1987.

Walsh, M. P., S. L. Bryant, R. S. Schechter, and L. W. Lake, Precipitation and dissolution of solids attending flow through porous media, *AIChE J.*, *30*(2), 317–328, 1984.

Westall, J. C., J. L. Zachary, and F. M. M. Morel, MINEQL: A computer program for the calculation of chemical equilibrium composition of aqueous systems, *Tech. Note 18*, 91 pp., Dept. of Civ. Eng., Mass. Inst. of Technol., Cambridge, 1976.

White, N., and L. W. Zelazny, Charge properties in soil colloids, in *Soil Physical Chemistry*, edited by D. L. Sparks, CRC Press, Boca Raton, Fla., 1986.

Yeh, G. T., D. D. Huff, FEMA: A finite element model of material transport through aquifers, *Rep. ORNL-6063*, Oak Ridge Natl. Lab., Oak Ridge, Tenn., 1985.

Yeh, G. T., and V. S. Tripathi, A critical evaluation of recent developments in hydrogeochemical transport models of reactive [illegible] 1989.

Yeh, G. T., and V. S. Tripathi, HYDROGEOCHEM: A coupled model of hydrological and geochemical equilibrium of multicomponent systems, *Rep. ORNL-6371*, Oak Ridge Natl. Lab., Oak Ridge, Tenn., 1990.

Yeh, G. T., and V. S. Tripathi, A model for simulating transport of reactive multispecies components: Model development and demonstration, *Water Resour. Res.*, *27*(12), 3075–3094, 1991.

J. Šimůnek and D. S. Suarez, U.S. Salinity Laboratory, Agricultural Research Service, U.S. Department of Agriculture, 4500 Glenwood Drive, Riverside, CA 92501.

(received February 3, 1993; revised October 12, 1993; accepted November 24, 1993.)